Title

Osteonecrosis of the Jaw Developed in Mice DISEASE VARIANTS REGULATED BY γδ T CELLS IN ORAL MUCOSAL BARRIER IMMUNITY*

Journal

Journal of Biological Chemistry, 290(28)

ISSN

0021-9258

Authors

Park, Sil
Kanayama, Keiichi
Kaur, Kawaljit
et al.

Publication Date

2015-07-01

DOI

10.1074/jbc.m115.652305

Peer reviewed

THE JOURNAL OF BIOLOGICAL CHEMISTRY VOL. 290, NO. 28, pp. 17349–17366, July 10, 2015

Osteonecrosis of the Jaw Developed in Mice

*DISEASE VARIANTS REGULATED BY γδ T CELLS IN ORAL MUCOSAL BARRIER IMMUNITY**

Received for publication, March 16, 2015, and in revised form, May 6, 2015 Published, JBC Papers in Press, May 26, 2015, DOI 10.1074/jbc.M115.652305

Sil Park[‡§], Keiichi Kanayama[‡¶], Kawaljit Kaur[§], Han-Ching Helen Tseng[§], Sina Banankhah[‡], Davood Talebi Quje[‡], James W. Sayre[‖], Anahid Jewett[§], and Ichiro Nishimura[‡§1]

From the [‡]Weintraub Center for Reconstructive Biotechnology, Division of Advanced Prosthodontics and [§]Division of Oral Biology and Medicine, UCLA School of Dentistry, Los Angeles, California 90095, the [¶]Department of Periodontology, Asahi University School of Dentistry, Gifu 501-0296, Japan, and the [‖]Department of Biostatistics, UCLA Fielding School of Public Health, Los Angeles, California 90095

Background: The pathological mechanism of osteonecrosis of the jaw (ONJ) is unknown.
Results: Mouse ONJ-like lesions exhibited epithelial hyperplasia associated with γδ T cells of mouse or human origin.
Conclusion: γδ T cells may modify the oral disease phenotypes of ONJ.
Significance: ONJ pathogenesis may involve multiple mechanisms separately leading to the development of osteonecrosis or oral epithelial abnormality.

Osteonecrosis of the jaw (ONJ), an uncommon co-morbidity in patients treated with bisphosphonates (BP), occurs in the segment of jawbone interfacing oral mucosa. This study aimed to investigate a role of oral mucosal barrier γδ T cells in the pathogenesis of ONJ. Female C57Bl/6J (B6) mice received a bolus zoledronate intravenous injection (ZOL, 540 μg/kg), and their maxillary left first molars were extracted 1 week later. ZOL-treated mice (WT ZOL) delayed oral wound healing with patent open wounds 4 weeks after tooth extraction with characteristic oral epithelial hyperplasia. γδ T cells appeared within the tooth extraction site and hyperplastic epithelium in WT ZOL mice. In ZOL-treated γδ T cell null (*Tcrd*$^{-/-}$ ZOL) mice, the tooth extraction open wound progressively closed; however, histological ONJ-like lesions were identified in 75 and 60% of WT ZOL and *Tcrd*$^{-/-}$ ZOL mice, respectively. Although the bone exposure phenotype of ONJ was predominantly observed in WT ZOL mice, *Tcrd*$^{-/-}$ ZOL mice developed the pustule/fistula disease phenotype. We further addressed the role of γδ T cells from human peripheral blood (h-γδ T cells). When co-cultured with ZOL-pretreated human osteoclasts *in vitro*, h-γδ T cells exhibited rapid expansion and robust IFN-γ secretion. When h-γδ T cells were injected into ZOL-treated immunodeficient (*Rag2*$^{-/-}$ ZOL) mice, the oral epithelial hyperplasia developed. However, *Rag2*$^{-/-}$ ZOL mice did not develop osteonecrosis. The results indicate that γδ T cells are unlikely to influence the core osteonecrosis mechanism; however, they may serve as a critical modifier contributing to the different oral mucosal disease variations of ONJ.

Osteonecrosis of the jaw (ONJ)[2] in the maxilla and mandible has emerged as an uncommon and occasionally severe co-morbidity among patients treated with a group of anti-resorptive agents such as amino-bisphosphonates (BP) (1) and denosumab, a humanized anti-RANKL monoclonal antibody (2). By contrast, ONJ has not been reported in patients treated with hormone replacement therapy or selective estrogen receptor modulators. ONJ is initially defined as an exposed jawbone in the oral cavity for more than 8 weeks even after appropriate intervention therapies in patients with current or past BP treatment (3, 4). An increasing number of case reports suggest that considerable variations exist in the clinical manifestations of ONJ, ranging from radiographic bone pathology without ulcerative oral mucosal lesions to localized swelling with persistent fistula formation (5–7).

ONJ is most frequently reported in zoledronate (ZOL)-treated patients with a primary diagnosis of multiple myeloma or bone metastatic tumors such as breast cancer (8, 9). These high risk patients are generally middle-aged to elderly, and they are often treated with immunosuppressive and chemotherapeutic agents, glucocorticoids, or both (10, 11). Therefore, other studies have addressed the combinatory effect of BP with multiple medications on the development of ONJ-like lesions in mice (Table 1). Although additional systemic and poly-pharmaceutical conditions might act as important cofactors that increase the prevalence of ONJ and contribute to its clinical variations (12, 13), the complex conditions have made it difficult to determine its core pathological mechanism.

ONJ primarily occurs in the oral segment of the jawbone that is tightly covered by keratinized oral mucosa. The oral mucosa, *i.e.* gingiva or palatal tissue, is composed of stratified epithelium and thin connective tissue; furthermore, it is considered to be

* This work was supported, in whole or in part, by National Institutes of Health Grant R01 DE022552 from NIDCR and was conducted in part in a facility supported by National Institutes of Health Grant C06 RR014529 from the National Center for Research Resources Research Facilities Improvement Program Grant. This work was also supported by Investigator Initiated Study Program Grant 38519 from Merck. The authors declare that they have no conflicts of interest with the contents of this article.

[1] To whom correspondence should be addressed: The Weintraub Center for Reconstructive Biotechnology, UCLA School of Dentistry, Box 951668, CHS B3-087, Los Angeles, CA 90095. Tel.: 310-794-7612; Fax: 310-825-6345; E-mail: inishimura@dentistry.ucla.edu.

[2] The abbreviations used are: ONJ, osteonecrosis of the jaw; BP bisphosphonate; ZOL, zoledronate; RANKL, receptor activator of NF-κB ligand; OC, osteoclast; h-OC, human osteoclast; pAg, phosphoantigen; IPP, isopentenyl pyrophosphate; m-OC, mouse OC; PEH, pseudoepitheliomatous hyperplasia; micro-CT, micro-computed tomography; PE, phycoerythrin; rh, recombinant human.

TABLE 1

ZOL doses in the mouse ONJ models

The following abbreviations are used: ZOL, zoledronate; Dex, dexamethasone; MEL, melphalan; s.c., subcutaneous injection; i.v., intravenous injection.

Mouse strain	Cumulative ZOL dose prior to oral manipulation	Single ZOL dose/injection	Study period of ZOL injection and oral manipulation	ONJ prevalence of the ZOL group alone	ONJ prevalence (systemic manipulation)	Ref.
	μg/kg	*μg/kg*				
Not reported	700 (300)	50 (s.c.)	3 weeks before and 4 weeks after tooth extraction	0%	0% (Dex 2.5 mg/kg) 0% (ZOL + Dex) 0% (MEL 3.5 mg/kg) 80% (ZOL + MEL)	46
C57Bl/6J	750–2000 (250)	125 (i.v.)	1 week before and 2 and 7 weeks after tooth extraction	17%	50% (Dex 5 mg/kg) 50% (ZOL + Dex)	47
C57Bl/6J	1300–3750 (750)	125 (i.v.)	3 weeks before and 3 and 12 weeks after tooth extraction	Not reported	Not reported ("The area of dead bone in the ZOL group was lower than that observed in the ZOL + Dex group")	48
C57Bl/6J	750 (250)	125 (i.v.)	1 week before and 2 weeks after tooth extraction	20%	45% (ZOL + Dex)	49
C57Bl/6J	600 (250)	125 (i.v.)	1 week before and 2 weeks after tooth extraction	Not reported	None	44
Beige nude/nude Xid	600 (250)	125 (i.v.)		Not reported	80% (5TGM cell infusion)	
C57Bl/6J	600 (600)	200 (i.v.)	1 week before and 7 weeks after dental pulp exposure	33%	None	50
C57Bl/6J	2750 (1750)	250 (s.c.)	7 days before and 5 days after tooth extraction	0%	None	51

one of the most protective tissue barriers against physical and chemical damage, bacterial infection, and environmental stress (14). Case control studies of patients with ONJ have indicated an increased risk of developing this condition with tooth extraction or the use of ill-fitting removable dental prostheses (15, 16). These "event-related" oral conditions among BP-treated patients can lead to inflammation in the oral mucosa tissue that likely activates oral barrier immunity. Thus, we hypothesized that the close proximity of the jawbone to the oral mucosa enables the involvement of abnormally stimulated oral barrier immunity during ONJ pathogenesis.

T cells expressing canonical γδ T cell receptors represent a small subset of circulating immune cells and account for 2–5% of peripheral blood T cells in humans. A deficiency in circulating γδ T cells has been reported in patients with long term and repeated BP administrations (17, 18), and BP-induced γδ T cell deficiency was postulated to promote an underlying susceptibility to the development of ONJ (17). Because γδ T cells are preferentially involved in barrier immunity (19, 20), we hypothesized that the γδ T cells in the oral barrier tissue play an important role in the development of ONJ. This study developed a mouse model exhibiting ONJ-like lesions. The role of γδ T cells was addressed in the γδ T cell-deficient *Tcrd*$^{-/-}$ mice and human γδ T cell-injected *Rag2*$^{-/-}$ mice. This study suggests that γδ T cells may not be centrally involved in its core osteonecrosis mechanism; however, their presence or absence in oral barrier immunity appears to contribute to the epithelial disease variations of ONJ.

Materials and Methods

Ethics Statement—The UCLA Animal Research Committee reviewed and approved all experimental protocols involving animals (ARC 1997-136). The UCLA Institutional Review Board reviewed and approved all protocols involving human subjects (IRB 12-001176).

ZOL Injection to Mice—This study sought to establish a mouse model exhibiting ONJ-like lesions. Seven-week-old female C57Bl/6J mice (the Jackson Laboratory, Bar Harbor, ME) were subjected to a bolus injection of 540 μg/kg ZOL (Reclast, Novartis, East Hanover, NJ) through the retro-orbital venous plexus (WT ZOL) (21). In the control group, 0.9% NaCl vehicle solution was injected through the retro-orbital venous plexus (WT NaCl). The ZOL dose, which is pharmacologically relevant to oncological doses in humans, was estimated via allometric scaling (22). Each mouse was administered only a single ZOL injection. In the initial study, mouse renal toxicity was evaluated using a creatinine clearance test for serum or urine samples obtained 1 day after ZOL ($n = 6$) or NaCl ($n = 6$) injection.

Maxillary First Molar Extraction—One week after the ZOL or NaCl injection, the maxillary left first molar was extracted (23). Mice were anesthetized via isoflurane inhalation and placed on a custom-made surgical table in a supine position using the fixed positioner on the maxillary incisors. A nasal tube was used for the continuous inhalation of 2–4% isoflurane mixed with oxygen during the surgical manipulations in the oral cavity. After the suprabony circumferential periodontal ligament of the attached gingiva was dissected with a dental explorer, the maxillary left first molar was laterally luxated by inserting the tip of a dental explorer between the first and second molars. The luxated molar was then gently removed using surgical forceps. Surgical complications such as tooth fracture occurred and appeared to cause confounding problems. As such, those mice were eliminated from further evaluation. Immediately prior to tooth extraction, 5.0 mg/kg carprofen was subcutaneously injected, and this injection was repeated every 24 h for 48 h.

Maxillary Tissue, Femur, and Whole Blood Collection—Euthanasia by 100% CO_2 inhalation was performed on day 4 (WT NaCl, $n = 6$; WT ZOL, $n = 7$), week 1 (WT NaCl, $n = 8$; WT ZOL, $n = 9$), week 2 (WT NaCl, $n = 11$; WT ZOL, $n = 11$), or week 4 (WT NaCl, $n = 8$; WT ZOL, $n = 12$) after tooth extraction. The maxilla containing the tooth extraction wound

and femur were harvested. The maxillary tissue was subjected to standardized digital photo recording. The clinical photograph was enlarged and examined for tooth extraction wound healing.

The harvested maxillary tissue and femurs were fixed in 10% buffered formalin and used for imaging by micro-computed tomography (micro-CT: μCT40, Scanco Medical, Bassersdorf, Switzerland) at an x-ray energy level of 55 peak kV with an intensity of 145 μA. The voxel size was 20 μm with a slice increment of 20 μm. The fixed maxillary tissues were further treated with a formic acid-based decalcifying solution (Immunocal, Ummunotec, Swanton, VT) or 10% EDTA for 7 days for histological section preparation as described below.

Separately, whole blood samples were obtained at the time of euthanasia via cardiac puncture using a 23-gauge needle. Serum chemistry was determined for alkaline phosphatase, calcium, and phosphorus (24).

Characterization of γδ T Cells in Mouse Oral Mucosal Tissue—To evaluate γδ T cells in the oral mucosa barrier tissue, a cell dissociation study was performed. Two weeks after molar extraction, the entire gingival/palatal oral mucosa tissue, including the wound area over the tooth extraction socket, was harvested from WT ZOL ($n = 3$) and WT NaCl ($n = 3$) mice. The gingival/palatal tissue was cut into small pieces, incubated with the premixed enzymes of a commercially available cell dissociation kit (Tumor Dissociation Kit, Miltenyi Biotec, Auburn, CA), and subjected to repeated mechanical agitations at room temperature and incubation at 37 °C. Dissociated gingival/palatal tissue cells were washed and incubated with FITC-conjugated monoclonal antibody against CD45 and PE-conjugated monoclonal antibodies against CD3, γδTCR (GL3), or DX5 (BioLegend, San Diego). IgG2b was used as the isotype control. After 15 min of incubation on ice, cells were analyzed by flow cytometry (EPICS XL-MCL, Coulter, Miami, FL) (25, 26). The data were presented using the lymphocyte gate.

To further investigate the presence of γδ T cells in the tooth extraction socket histologically, Tcrd-H3BEGFP mice were used. Because of a knock-in mutation of an internal ribosome entry site-controlled histone 2B-enhanced GFP inserted into the 3′ end of the T cell receptor δ constant gene, γδ T cells of Tcrd-H2BEGFP mice were highlighted by GFP fluorescence (Tcrd- GFP^+) (25). Tcrd-H2BEGFP mice were subjected to ZOL or NaCl injection followed by maxillary first molar extraction as described above. At day 4 ($n = 3$ in each group) and week 2 ($n = 3$ in each group) of tooth extraction, the maxillary tissue was harvested. After being fixed in 10% buffered formalin and decalcified, maxillary tissues were embedded in paraffin. Deparaffinized frontal sections, including the tooth extraction site, were subjected to antigen retrieval via microwave irradiation and incubated with an anti-GFP antibody (Santa Cruz Biotechnology, Dallas). GFP^+ cells were visualized using the diaminobenzidine substrate, and the sections were counterstained with hematoxylin. Representative tooth extraction sockets were identified, and the number of GFP^+ cells within the socket was determined. The data are presented as the number of GFP^+ cells per extraction socket area (mm^2).

ONJ Development in γδ T Cell Null ($Tcrd^{-/-}$) Mice—γδ T cell null ($Tcrd^{-/-}$) mice carry T cell receptor Cδ that was disrupted by gene targeting, resulting in the loss of T cells with γδTCR expression in the lymphoid and epithelial tissues (27). To address the role of γδ T cells in the pathological development of ONJ, female 7-week-old $Tcrd^{-/-}$ mice (B6.129P2-$Tcrd^{tm1Mom}$/J, The Jackson Laboratory) were treated with a ZOL injection ($Tcrd^{-/-}$ ZOL) followed by maxillary first molar extraction as described above.

Because WT ZOL mice exhibited delayed tooth extraction healing and developed ONJ-like lesions at week 4, we primarily investigated the wound healing phenotype of $Tcrd^{-/-}$ ZOL mice at week 4 ($n = 15$). In addition, this study examined the early wound healing process of $Tcrd^{-/-}$ ZOL mice at day 4 ($n = 3$), week 1 ($n = 3$), and week 2 ($n = 6$). The harvested maxillary tissues were photo-recorded, fixed with 10% buffered formalin, and subjected to micro-CT imaging. The specimens were further subjected to decalcification and paraffin embedding for histological specimen preparation. In a parallel experiment, $Tcrd^{-/-}$ mice injected with 0.9% NaCl vehicle solution via the retro-orbital venous plexus were subject to left maxillary first molar extraction ($n = 6$). Maxillary tissue was harvested on week 2.

Evaluation of Oral Mucosa Inflammation—The digital photo-records from WT NaCl, WT ZOL, and $Tcrd^{-/-}$ ZOL mice were used to identify the presence or absence of clinical alveolar bone exposure of WT and $Tcrd^{-/-}$ mice. The swelling area of gingival/palatal tissue was measured using a Java-based image-processing program (ImageJ, National Institutes of Health, Bethesda), which was standardized using the circumferential crown area of the remaining first molar.

To assess the inflammation degree of the oral mucosal tissue, cells dissociated from gingival/palatal tissues harvested at day 4 and week 2 ($n = 3$ in each group) were incubated with a PE-conjugated CD45 monoclonal antibody (BioLegend) and analyzed using flow cytometry. The number of $CD45^+$ lymphocytes among the total cells dissociated from gingival/palatal tissues was determined.

Histological Examination of ONJ-like Lesions—The fixed and decalcified maxillary tissues of WT NaCl, WT ZOL, and $Tcrd^{-/-}$ ZOL mice were subjected to a conventional paraffin-embedded histological preparation. A series of frontal sections (8 μm thick) of maxilla were prepared by bisecting the tooth extraction site and the contralateral remaining first molar. Histological sections were stained with hematoxylin and eosin. Histological images were digitized using a high throughput imaging system (Ariol SL-50, Applied Imaging, Grand Rapids, MI) and archived. ONJ-like lesions were determined based on the following criteria following the updated ONJ definition by the American Association of Oral and Maxillofacial Surgeons (28): 1) jawbone exposure associated with abnormal epithelial hyperplasia communicating to the palatal/alveolar bone, or 2) the development of a pustule directly on the surface of the alveolar bone associated with epithelial fistula. The jawbone exposure exhibited food and debris impaction, whereas the pustule only contained inflammatory cells. The prevalence was expressed as the number of animals with ONJ-like oral mucosal abnormalities over the number of animals at week 4.

For alveolar bone characterization, the histological images of palatal/alveolar bone containing the first molar extraction site

were horizontally bisected to divide the oral and nasal sides. The primary focus was placed on the oral side of palatal/alveolar bone, which encompassed the buccal border of the alveolar bone to the mid-palatine suture. The degree of osteonecrosis was defined as the ratio between the number of osteocytes and the number of nonvital osteocytes determined using osteocytic lacunae without a cellular component (*i.e.* empty lacunae) or abnormally condensed small nuclei (pyknotic osteocytes). An operator blind to condition performed the histological evaluation.

The number of osteoclasts (OCs) within the oral half of the palatal/alveolar bone containing the first molar extraction site was counted in the histological specimens under ×20 magnification. OCs were defined as large cells with multiple nuclei (≥2 nuclei) on the bone surface. Specific histological sections were stained with tartrate-resistant acid phosphatase using a commercially available kit (Sigma). The area of palatal/alveolar bone was measured using an image-processing program (ImageJ, National Institutes of Health). The OC number was normalized to the palatal/alveolar bone area.

Micro-CT Examination—Micro-CT data were reconstructed to generate three-dimensional images at a threshold of 220 using the software provided by the manufacturer of the micro-CT scanner.

Maxillary micro-CT three-dimensional images of WT NaCl, WT ZOL, and *Tcrd*$^{-/-}$ ZOL mice were used to identify alveolar bone abnormalities such as periosteal reaction, bone sequestra associated with ONJ, and bone remodeling. A blinded operator reviewed the micro-CT three-dimensional images, and the degrees of bone formation and bone resorption at the tooth extraction site were separately rated from 0 to 2. The bone remodeling index was calculated by combining the bone formation and resorption indices. Various micro-CT images exhibited severe periosteal reactions at the external surface of the alveolar bone, which were not considered in the quantitative evaluation.

Bone morphometry of femurs harvested 2 weeks after tooth extraction or 3 weeks after ZOL injection was characterized in WT NaCl, WT ZOL, and *Tcrd*$^{-/-}$ ZOL mice ($n = 6$ in each group) by micro-CT. Volume of interest was set 600 μm below the end point of the growth plate, which was used as an anatomical landmark. One hundred slices (1.2 mm) were evaluated in the distal femur metaphysis at a threshold of 220. The volume of interest only included secondary spongiosa. Trabecular bone morphometric measurements in three-dimensions included the following: bone volume normalized to tissue volume, trabecular number, trabecular thickness, and trabecular separation.

Human γδ T Cells and CD3$^+$ T Cells Co-cultured with ZOL-pretreated Human Osteoclasts—For preparing human osteoclasts (h-OCs), peripheral blood was collected from healthy donors, and peripheral blood mononuclear cells were separated by Ficoll-Hypaque gradient centrifugation. Peripheral blood mononuclear cells were cultured onto the tissue culture plate for 1 h, after which the adherent subpopulation of peripheral blood mononuclear cells was detached from the tissue culture plates, and the CD14$^+$ monocytes were purified (EasyStep Human Monocyte Isolation Kit, Stem Cell Technologies, Vancouver, Canada). Approximately 94% purity was achieved based on flow cytometric analysis of CD14. Monocytes (10.3×10^6 cells) were cultured in α-minimal essential medium containing 25 ng/ml macrophage colony-stimulating factor (M-CSF) and receptor activator of nuclear factor-κB ligand (RANKL) (25 ng/ml) (29). Medium was refreshed every 3 days. Development of h-OCs was monitored by tartrate-resistant acid phosphatase staining (Primary Cell Co., Sapporo, Japan) and resorption pit formation on synthetic carbonate apatite pre-coated plate (Cosmo Bio USA, Carlsbad, CA) following the manufacturer's protocols. Mature h-OCs were generated after 14–21 days of incubation. Once developed, h-OCs were treated with 100 nM ZOL for 6 days.

For preparing human γδ T cells and CD3$^+$ T cells (h-γδ T cells and h-CD3$^+$ T cells, respectively), peripheral blood samples of healthy donors were used to purify the corresponding cells by commercially available selection kits (EasyStep Human Gamma/Delta T Cell Isolation kit and EasyStep Human CD3 Positive Selection kit, StemCell Technologies). As the result, h-γδ T cells (3.0×10^9) and h-CD3$^+$ T cells (51×10^9 cells), respectively, were obtained. h-γδ T and h-CD3$^+$ T cells were activated in RPMI 1640 media containing anti-CD3 antibody (1 μg/ml), anti-CD28 antibody (7 μg/ml), and rh-IL-2 (100 units/ml) overnight. Then, h-γδ T cells (3.0×10^9 cells per plate) and h-CD3$^+$ T cells (16.3×10^9 cells per plate) were co-cultured with ZOL-pretreated h-OCs (0.6×10^9 and 2.0×10^9 cells per plate, respectively).

The number of h-γδ T and h-CD3$^+$ T cells in each plate was counted at co-culture days 1, 3, and 6. The co-culture medium of h-OC/h-γδ T cells and h-OC/h-CD3$^+$ T cells was harvested at day 6, and IFN-γ concentration was determined by ELISA. h-γδ T cells were then collected, washed with PBS, and prepared for injection to the *Rag2*$^{-/-}$ mouse as described below. On the day of mouse injection, surface markers of h-γδ T cells were analyzed by flow cytometry using PE-conjugated monoclonal anti-human CD3, CD4, CD19, and CD69 antibodies (BioLegend) (25, 26).

ONJ Development in B/T Cell-deficient (Rag2$^{-/-}$*) Mice and the Effect of h-γδ T Cell Repopulation—Rag2*$^{-/-}$ mice (B6(Cg)-*Rag2tm1.1Cgn*/J, The Jackson Laboratory) carry null mutation in recombination-activating gene-2 resulting in the deficiency of B and T lymphocytes (30). Female WT mice and *Rag2*$^{-/-}$ mice received the single injection of 500 μg/kg ZOL (WT ZOL and *Rag2*$^{-/-}$ ZOL, respectively) or 0.9% NaCl vehicle solution (WT NaCl and *Rag2*$^{-/-}$ NaCl, respectively) via tail vein. In this experiment, mice were housed with autoclaved cellulose-based bedding (Cell-Sorb Plus, Fangman Specialties Inc., Cincinnati, OH).

Maxillary tissue containing the tooth extraction site was photographed and harvested. After being fixed and decalcified, the conventional histological preparation as described above was stained with H&E.

Six days after the ZOL injection, a group of *Rag2*$^{-/-}$ ZOL mice ($n = 4$) was injected via tail vein with h-γδ T cells (6.75×10^9 per mouse) that had been activated by anti-CD3 and anti-CD28 antibodies and rh-IL-2 followed by co-culturing with ZOL-pretreated h-OCs as described above (*Rag2*$^{-/-}$ ZOL h-γδ T cell). One day after the h-γδ T cell injection (*Rag2*$^{-/-}$ ZOL h-γδ T cell, $n = 4$) or 1 week after ZOL injection (WT ZOL, $n =$

5; *Rag2*$^{-/-}$ ZOL, $n = 4$; WT NaCl, $n = 4$; *Rag2*$^{-/-}$ NaCl, $n = 4$), the maxillary first molar was extracted.

All mice were euthanized 2 weeks after tooth extraction. Spleens and bone marrow cells were harvested from *Rag2*$^{-/-}$ ZOL h-γδ T cell mice. Splenocytes and bone marrow cells were incubated with FITC-conjugated monoclonal antibody against mouse CD45 and PE-conjugated monoclonal antibodies against mouse γδTCR (GL3), CD19, DX5, or F4/80 (BioLegend). Furthermore, splenocytes and bone marrow cells were incubated with FITC-conjugated monoclonal antibodies against human CD45 or CD3 and PE-conjugated monoclonal antibodies against human γδTCR, CD19, or NkP46 (BioLegend) and analyzed by flow cytometry. IgG2b served as the isotype control.

Using histological sections stained with H&E, osteonecrosis was assessed by the cluster area of ≥5 necrotic osteocytes over the alveolar bone area. Epithelial abnormality was assessed for the presence or absence of hyperplastic epithelium.

Standardized Osteoclast Number of WT and Rag2$^{-/-}$ *Mice*—The histological sections through the distal root area of the first molar from the above experiment were stained by tartrate-resistant acid phosphatase, and the number of OCs on the surface of palatal bone and in the tooth extraction socket was separately counted. The number of OC was standardized by the bone surface linear length.

Effect of m-OC on h-γδ T Cell and Mouse (m)-γδ T Cells in Vitro—m-OCs were generated from mouse femur flow-through cells with supplementation with 25 ng/ml M-CSF and 25 ng/ml RANKL for 7 days. h-γδ T cells were isolated from peripheral blood of healthy subjects as described above. m-γδ T cells were isolated from mouse spleen (TCRγ/δ T cell isolation kit, mouse, Miltenyi Biotec). After the activation with rh-IL2 (100 units/ml) and lipopolysaccharide (LPS) (100 ng/ml), h-γδ T cells and m-γδ T cells were co-cultured with m-OCs that were exposed to 100 nM ZOL for overnight. h-γδ T cells and m-γδ T cells were also co-cultured with m-OCs without ZOL pretreatment. At 1, 4, and 8 days of co-culture, the medium was collected and assayed for IFN-γ by ELISA.

Statistical Analyses—Student's *t* tests were used to compare means. A one-way analysis of variance followed by a Bonferroni correction was used when more than two groups were compared. Fisher's exact test was used to describe the prevalence of ONJ-like lesions in contingency tables. The correlation between osteonecrosis and OC numbers was assessed by Pearson correlation and Spearman's rank correlation tests.

Results

ONJ-like Lesions in WT Mice—In control WT mice injected with 0.9% NaCl vehicle solution (WT NaCl), the maxillary first molar extraction created an open wound the size of the maxillary first molar crown, which remained open after surgery. Four days after tooth extraction, all WT NaCl mice continued to exhibit an open wound in the gingival tissue, which was surrounded by localized swelling (Fig. 1*A*). The open wound of the maxillary gingival tissue progressively closed and was completely covered by epithelial tissue between weeks 2 and 4. In the ZOL-treated WT mice (WT ZOL), the closure of gingival open wounds was slow. In total, 50% (6/12) of the animals exhibited clinically open wounds at week 4, and the soft tissue swelling continued to surround the wound opening (Fig. 1*A*). The open wound was more common at the large mesial root, which was observed in all WT ZOL mice.

Histological sections revealed that the tooth extraction wounds of WT NaCl mice healed with new bone formation in the bony socket, and the oral epithelial integrity was re-established between weeks 2 and 4 (Fig. 1*B*). Mild inflammatory cell infiltrates were observed in the palatal oral mucosa. By contrast, WT ZOL mice exhibited alveolar bone exposure at the mesial root extraction site with food and debris impaction. At the small distal root areas, where the oral mucosa wound was closed based on gross observation, histological evaluations revealed definitive bone exposure facilitated by the abnormal migration of oral epithelial cells. The abnormal proliferation and migration of epithelial cells resembling pseudoepitheliomatous hyperplasia (24, 31) resulted in direct epithelial contact with the partially necrotic alveolar bone. Reduced new bone formation was noted in the extraction socket, and densely localized inflammatory cell infiltration was observed on the surface of the palatal bone adjacent to the tooth extraction site (Fig. 1*B*).

WT NaCl and WT ZOL mice showed serum levels of alkaline phosphatase (125.7 ± 29.95 and 97.0 ± 28.36 units/liter, respectively), calcium (8.9 ± 0.61 and 9.1 ± 0.88 mg/dl, respectively), and phosphorus (8.4 ± 1.44 and 7.0 ± 2.59 mg/dl, respectively). These serum chemistry data did not indicate any differences between groups and were within the normal range, *i.e.* alkaline phosphatase, 13–291 units/liter; calcium, 6.8–11.9 mg/dl, and phosphorus, 5.3–11.3 mg/dl. Furthermore, WT NaCl and WT ZOL mice exhibited similar renal function as measured by creatinine clearance (0.35 ± 0.07 and 0.33 ± 0.01 mg/dl, respectively), which was within the normal range of 0.1–2.1 mg/dl. No signs of toxicity related to ZOL injection were observed.

Oral γδ T Cells in the Tooth Extraction Wound—The cellular component was dissociated from gingival/palatal oral mucosa tissues harvested from WT NaCl and WT ZOL mice 2 weeks after the tooth extraction. Cells in the lymphocyte gate in the flow cytometry were predominantly composed of CD45$^+$ cells (Fig. 2*A*). Within the CD45$^+$ population, the WT NaCl and WT ZOL samples contained 7.1 and 5.5% CD3$^+$ T cells, respectively. GL3$^+$ γδ T cells were 0.4 and 1.3%, and DX5$^+$ natural killer cells were 1.1 and 2.3% in the WT NaCl and WT ZOL samples, respectively. It was estimated that the fraction of γδ T cells in the infiltrated T cell population was 5.6 and 23.6% in the WT NaCl and WT ZOL oral wound samples at week 2 of tooth extraction.

Using Tcrd-H2BEGFP mice, GFP$^+$ γδ T cells were examined in the extraction socket (Fig. 2*B*). At day 4 after tooth extraction, the number of GFP$^+$ γδ T cells did not differ between Tcrd-H2BEGFP NaCl and ZOL mice (Fig. 2*C*). However, at week 2 of wound healing, the number of GFP$^+$ γδ T cells significantly decreased in the control mice. By contrast, Tcrd-H2BEGFP ZOL mice exhibited an increase of GFP$^+$ γδ T cells in the tooth extraction socket (Fig. 2*C*). A few GFP$^+$ γδ T cells were identified in the unwounded junctional epithelium of the free gingiva adjacent to the tooth (Fig. 2*D*). However, in the oral epithelial hyperplasia in Tcrd-H2BEGFP ZOL mice, an

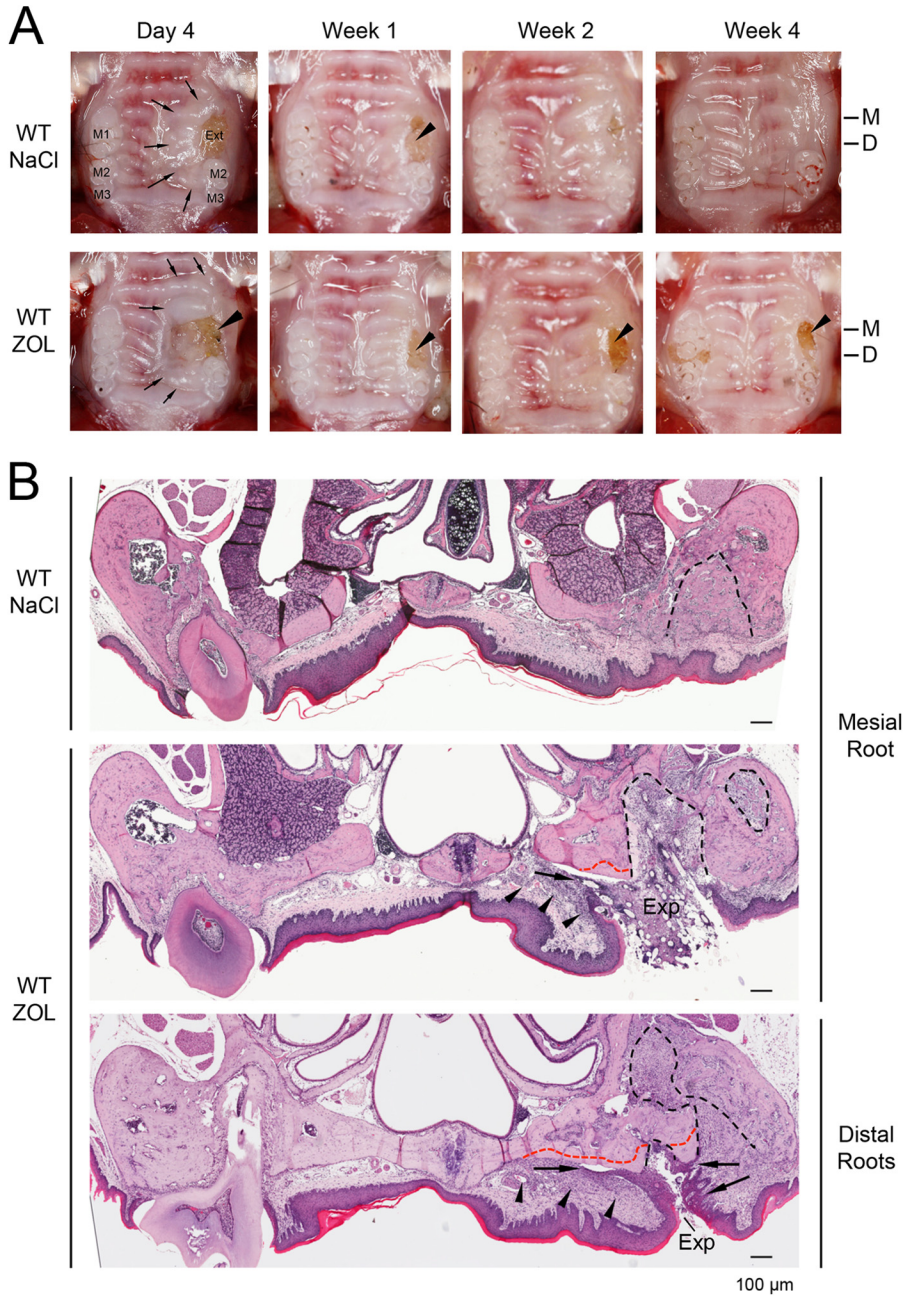

FIGURE 1. **Tooth extraction wound healing in WT mice and the development of ONJ-like lesions in ZOL-treated WT mice (WT ZOL).** *A,* time course of gingival/palatal tissue healing after maxillary first molar extraction (*Ext*). For control mice receiving 0.9% NaCl vehicle injection (*WT NaCl*), the open wound and surrounding tissue swelling (*arrows*) were progressively reduced from day 4 to week 2 after tooth extraction and healed by week 4. Mice administered a 540 μg/kg ZOL injection (*WT ZOL*) demonstrated slow wound healing, leaving the tooth extraction open wound (*arrowheads*) unclosed at the mesial root (*M*) with lesser degrees at the distal roots (*D*). The swelling of the gingival/palatal tissue (*arrows*) was restricted to the tooth extraction side. *B,* histological evaluations of tooth extraction wounds in WT NaCl and WT ZOL mice at week 4. Control WT NaCl mice exhibited complete wound healing as demonstrated by an extraction socket (*black dotted line*) filled with new bone formation and the re-establishment of oral epithelial integrity. The extraction wound was not closed in WT ZOL mice, enabling food and debris impaction. The jawbone exposure (*Exp*) was severe in the mesial root site; however, the distal root site revealed minimal but definitive jawbone exposure associated with abnormal epithelial growth resembling PEH (*arrows*). The tooth extraction socket (*black dotted line*) exhibited delayed bone formation. Osteonecrosis (*red dotted line*) was observed at the bone exposure site as well as the surface of the palatal/alveolar bone interfacing the oral mucosa with a localized dense inflammatory cell infiltration (*arrowheads*).

increased density of GFP^+ γδ T cells was observed (Fig. 2*D*). Combining the data of $GL3^+$ and GFP^+ γδ T cells, ZOL treatment appeared to associate with the sustained appearance of γδ T cells in the oral mucosa at the tooth extraction wound site.

Different Oral Mucosa Wound Healing in $Tcrd^{-/-}$ ZOL Mice—We addressed the possible role of γδ T cells in the development of ONJ using γδ T cell-deficient ($Tcrd^{-/-}$) mice. The healing patterns of the tooth extraction wound were indistinguishable between the WT ZOL and $Tcrd^{-/-}$ ZOL mice until week 1. At week 2, the tooth extraction wound area was visibly reduced in $Tcrd^{-/-}$ ZOL mice compared with WT ZOL mice. At week 4, the tooth extraction wound was closed in 86.7% of $Tcrd^{-/-}$ ZOL mice (13/15); however, gingival/palatal tissue swelling remained (Fig. 3*A*). The standardized oral mucosal

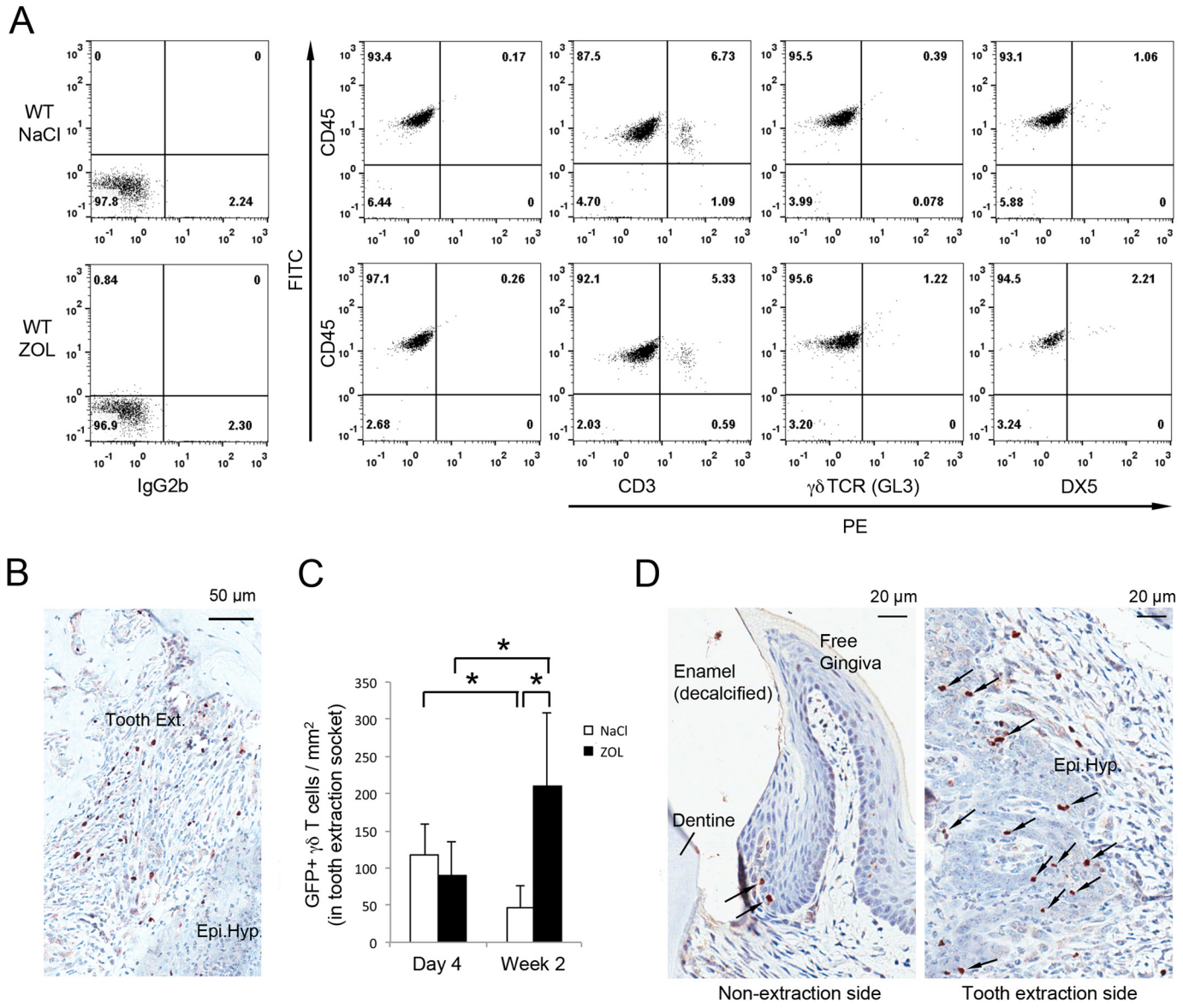

FIGURE 2. **Appearance of γδ T cells in the oral mucosa after tooth extraction.** *A,* palatal/gingival tissue of WT NaCl or WT ZOL mice was harvested 2 weeks after tooth extraction, and cells were dissociated by repeated enzymic digestions. Dissociated cells were incubated with CD45, CD3, γδTCR (GL3), or DX5 antibodies and examined by flow cytometry. In a representative analysis, $CD45^+$ population contained $CD3^+$ T cells at similar rates; however, the WT ZOL sample showed higher levels of $GL3^+$ γδ T cells and $DX5^+$ NK cells than the WT NaCl sample. *B,* to further identify γδ T cells, maxillary histological specimens were prepared from NaCl or ZOL-injected Tcrd-H2BEGFP mice 4 days or 2 weeks after tooth extraction (*Ext.*). Anti-GFP antibody was used to highlight GFP^+ γδ T cells by immunohistology. A cluster of GFP^+ γδ T cells was found in the connective tissue of the tooth extraction wound. *C,* number of GFP^+ γδ T cells in the tooth extraction socket was found to be similar 4 days after tooth extraction in WT NaCl ($n = 4$) and WT ZOL ($n = 4$) mice. However, although in the control WT NaCl mice ($n = 4$), GFP^+ γδ T cells decreased 2 weeks after tooth extraction, the GFP^+ γδ T cell number increased in WT ZOL mice ($n = 4$). *, $p < 0.05$ *D,* in some WT ZOL mice, PEH-like oral epithelial hyperplasia (*Epi Hyp*) was observed at the tooth extraction site. GFP^+ γδ T cells were abundant in the hyperplastic epithelium but not in normal oral epithelium.

swelling area was significantly larger in the $Tcrd^{-/-}$ ZOL mice compared with the WT ZOL mice at weeks 2 and 4 (Fig. 3*B*).

Pustule/Fistula Development on the Necrotic Bone Surface of $Tcrd^{-/-}$ ZOL Mice—Histological cross-sections of $Tcrd^{-/-}$ ZOL mice revealed well healed extraction sockets and oral mucosa wounds at week 4 (Fig. 3*C*). In 26.7% of the $Tcrd^{-/-}$ ZOL mice, small sequestrations of necrotic bone were observed in the connective tissue of the oral mucosa. Unlike the ONJ-like lesions of the WT ZOL mice, the development of large pustules on the surface of necrotic palatal bones was observed in $Tcrd^{-/-}$ ZOL mice (Fig. 3*C*). The associated epithelium at the pustule was consistent with fistula formation.

Prevalence of ONJ-like Lesions in WT NaCl, WT ZOL, and $Tcrd^{-/-}$ ZOL Mice—Histological jawbone exposure was observed in both the WT ZOL (66.7%) and $Tcrd^{-/-}$ ZOL (20.0%) groups (Fig. 3*D*). By contrast, pustule/fistula formation was predominantly observed in $Tcrd^{-/-}$ ZOL mice (40.0%) compared with WT ZOL mice (8.3%), although this was not significant ($p = 0.06$). When the bone exposure phenotype and pustule/fistula phenotype were combined as ONJ, the WT ZOL (75.0%) and $Tcrd^{-/-}$ ZOL (60.0%) mice suggested an equal likelihood of developing ONJ-like lesions (Fig. 3*D*). The prevalence of oral epithelial abnormalities was 0% in WT NaCl control mice at week 4.

Oral Mucosal Disease Phenotypes of ONJ in Mice

The effect of ZOL on the femurs was characterized in WT ZOL and *Tcrd*$^{-/-}$ ZOL mice by micro-CT, which demonstrated the similar increases in bone volume normalized to tissue volume and trabecular number and decreases in trabecular separation as compared with the WT NaCl control group (Fig. 3*E*). No significant difference was noted between WT ZOL and *Tcrd*$^{-/-}$ ZOL femurs.

Severe Periosteal Reactions Occurred in WT ZOL Mice but Not in Tcrd$^{-/-}$ *ZOL Mice*—Radiographic and CT image examinations of patients with ONJ have revealed that periosteal reac-

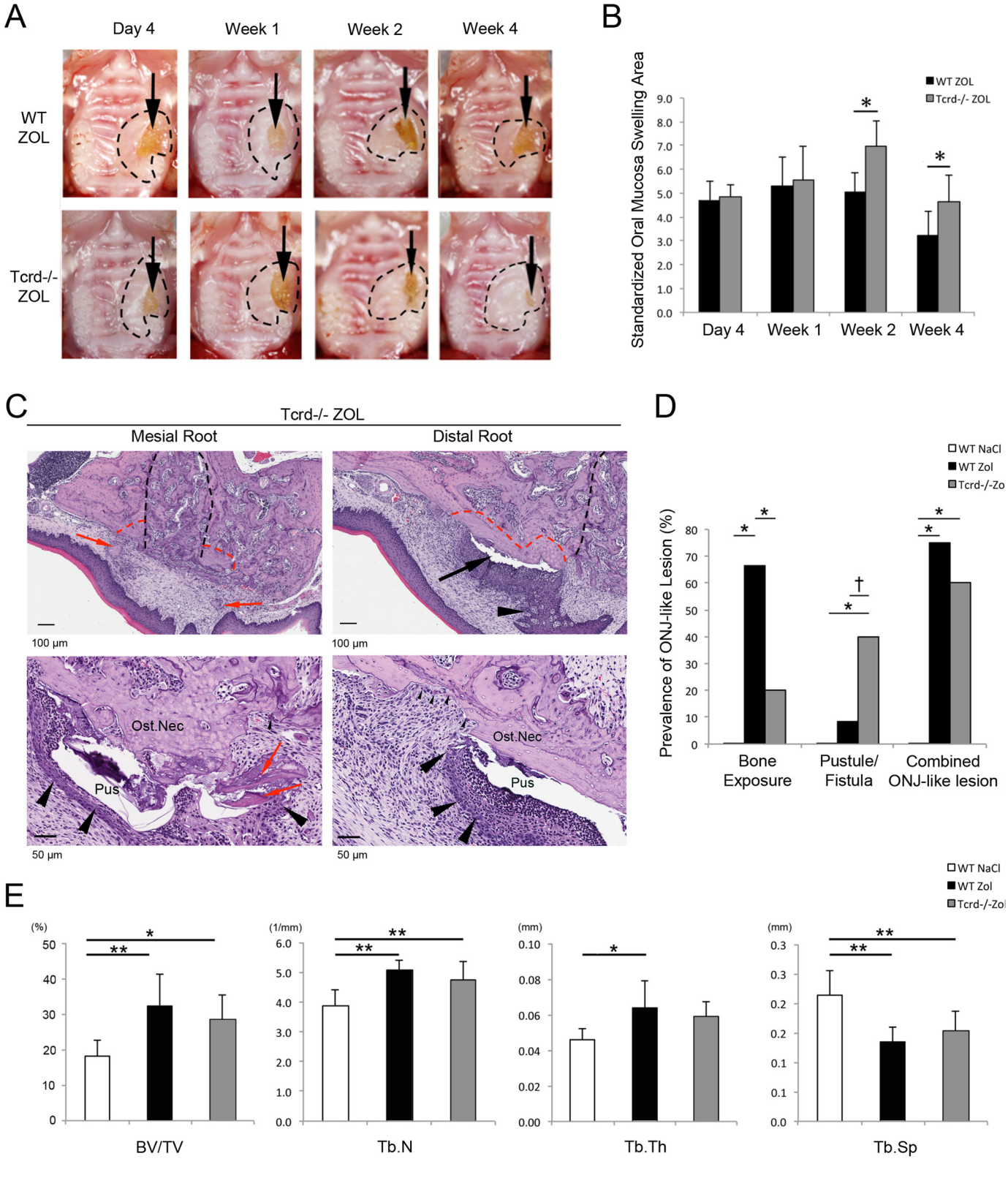

tion predominantly occurs during advanced disease stages (32, 33). This study used micro-CT images to determine the presence of abnormal alveolar bone in mouse maxilla. WT NaCl mice revealed evidence of bone resorption in the palatal alveolar bone at week 2 of tooth extraction as well as bone formation in the extraction socket at week 4 (Fig. 4, *A* and *B*). WT NaCl mice did not exhibit abnormal alveolar bone wound healing. ZOL treatment of WT and *Tcrd*$^{-/-}$ mice appeared to decrease osteolytic signs at the extraction site, whereas bone formation in the extraction socket was less affected (Fig. 4, *A* and *B*). A total of 53% of WT ZOL mouse specimens from weeks 2 and 4 exhibited periosteal reactions, including severe forms, at the tooth extraction wound healing site or the contralateral periodontal disease area (Fig. 4*A*). *Tcrd*$^{-/-}$ ZOL mice demonstrated a small "sun-ray" type of calcified spikes on the surface of the alveolar bone; however, the severity of the periosteal reaction was attenuated considerably (Fig. 4*A*).

Chronic Oral Mucosa Inflammation in WT ZOL and Tcrd$^{-/-}$ *ZOL Mice*—Oral epithelial hyperplasia in WT ZOL mice migrated toward the inflammatory lesion and established direct contact between the basal cells and the surface of partially necrotic alveolar bone (Fig. 5*A*). These characteristic features were less apparent in *Tcrd*$^{-/-}$ ZOL mice, and the epithelial tissue did not reach the bone surface except at the periphery of the pustule (Fig. 5*A*). Despite the different oral mucosal disease phenotypes of ONJ-like lesions in WT ZOL and *Tcrd*$^{-/-}$ ZOL mice, both models exhibited sustained inflammation. WT ZOL mice exhibited localized and dense inflammatory cell infiltrates near the bone surface, whereas inflammation in the gingival/palatal mucosa tissues was more diffuse and often exhibited cellulitis-like inflammatory cell infiltration in *Tcrd*$^{-/-}$ ZOL mice (Fig. 5*A*).

Dissociated cells from the gingival/palatal mucosa tissues contained over 50% CD45$^+$ leukocytes in both the WT NaCl and WT ZOL mice at day 4 (Fig. 5*B*). Control WT NaCl mice exhibited a significant reduction in CD45$^+$ cells at week 2, whereas WT ZOL mice maintained high levels of CD45$^+$ cells at week 2 (Fig. 5*B*). Similarly, *Tcrd*$^{-/-}$ ZOL mice exhibited an increase in CD45$^+$ cells at week 2 (Fig. 5*B*). Two weeks after the maxillary first molar extraction, *Tcrd*$^{-/-}$ NaCl mice also sustained oral mucosa swelling and CD45$^+$ cells infiltration (data not shown).

Osteonecrosis in WT ZOL and Tcrd$^{-/-}$ *ZOL Mice*—The degree of osteonecrosis in the palatal/alveolar bone was defined as the proportion of nonvital osteocyte lacunae in the oral and nasal sides. The nasal side of palatal bone contained 10–15% nonvital osteocyte lacunae in all groups at all of the tested time points (data not shown). The oral side of the palatal bone exhibited a cluster of ~20% nonvital osteocyte lacunae immediately after tooth extraction, which gradually decreased over time in control WT NaCl mice (Fig. 5*C*). In WT ZOL mice, the area of osteonecrosis was observed in the bone exposure site as well as the palatal bone that interfaced the oral mucosa and dense inflammatory infiltrates (Fig. 5*A*). The area of osteonecrosis was not reduced over time but rather increased at week 4, which resulted in persistent osteonecrosis (Fig. 5*C*). The osteonecrosis areas of the *Tcrd*$^{-/-}$ ZOL mice were associated with bone sequestra and pustules (Fig. 5*A*). The *Tcrd*$^{-/-}$ ZOL group exhibited increased osteonecrosis development at week 2, followed by a mild decrease at week 4 (Fig. 5*C*). The reference *Tcrd*$^{-/-}$ NaCl group developed a significantly smaller necrotic bone area at week 2, despite the remaining open wound (data not shown).

The number of OCs in the palatal/alveolar bone of WT NaCl control mice demonstrated an early increase at day 4 and week 1 after tooth extraction, followed by a gradual decrease (Fig. 5*D*). By contrast, OCs in the palatal/alveolar bone of WT ZOL and *Tcrd*$^{-/-}$ ZOL mice remained relatively unchanged throughout the experiment, resulting in a significantly increased number compared with the WT NaCl mice at week 4 (Fig. 5*D*). Active bone resorption was observed at the pustule periphery (Fig. 5*A*). The removal of necrotic bone sequestra might contribute to the late decrease of osteonecrosis area in *Tcrd*$^{-/-}$ ZOL mice.

The correlation between the area of osteonecrosis and the number of osteoclasts in the combined data of weeks 1, 2, and 4 was evaluated by Pearson correlation and Spearman's rank correlation tests. The WT NaCl group revealed the significant correlation in both tests, whereas the WT ZOL and *Tcrd*$^{-/-}$ ZOL groups showed a similar correlation pattern with no statistical significance (Fig. 5*E*).

In summary, ZOL-treated *Tcrd*$^{-/-}$ mice developed the different oral mucosa disease phenotype characterized by the pustule and fistula formation; however, the osteonecrosis occurred similarly to WT ZOL mice.

Activation of Human Peripheral Blood γδ T Cells by ZOL-pretreated h-OC—h-γδ T cells contain Vγ9Vδ2 T cells. BP-treated macrophages accumulate phosphorylated metabolites such as isopentenyl pyrophosphate (IPP) (34), which have been shown to selectively activate h-γδ T cells but not mouse γδ T cells. In the context of ONJ pathogenesis, we investigated the role of ZOL-treated h-OCs, rather than peripheral blood macrophages, on the activation of h-γδ T cells in this project.

Three million h-γδ T cells and 51 million h-CD3$^+$ T cells were isolated from approximately equal volumes of peripheral blood of different healthy donors. The estimated purity of h-γδ

FIGURE 3. **ONJ-like lesions in ZOL-treated γδ T cell null mice (*Tcrd*$^{-/-}$ ZOL).** *A,* tooth extraction created the open wound (*arrow*) in the oral mucosa, which became visibly and consistently smaller in *Tcrd*$^{-/-}$ ZOL mice compared with WT ZOL mice at week 4. The swelling remained in the gingival/palatal tissues in *Tcrd*$^{-/-}$ ZOL mice (*black dotted line*). *B,* area of swelling normalized by the circumferential crown size of the contralateral first molar was significantly increased in *Tcrd*$^{-/-}$ ZOL mice compared with WT ZOL mice at weeks 2 and 4; *, $p < 0.05$. *C,* histological examination revealed that *Tcrd*$^{-/-}$ ZOL mice did not exhibit the bone exposure as observed in WT ZOL mice. The development of pustule (*arrows*; *Pus*) associated with epithelial fistulation (*arrowheads*) was demonstrated. The tooth extraction socket (*black dotted line*) healed uneventfully and was filled with woven bone. Osteonecrosis (*red dotted line*; *Ost.Nec*) was observed at the pustule areas and bone sequestration (*red arrows*). *D,* prevalence of necrotic jawbone exposure was significantly higher in WT ZOL mice than *Tcrd*$^{-/-}$ ZOL or WT NaCl control mice. However, *Tcrd*$^{-/-}$ mice exhibited more pustule/fistula formation than WT ZOL and WT NaCl mice. Both ONJ phenotypic variants were combined, and the prevalence of ONJ-like lesion development was found indistinguishable between WT ZOL and *Tcrd*$^{-/-}$ ZOL mice. *, $p < 0.05$; †, $p = 0.06$. *E,* micro-CT characterization of femur trabecular bone morphology of WT NaCl, WT ZOL, and *Tcrd*$^{-/-}$ ZOL mice. The effect of ZOL was shown as the increased bone mass and structure of trabecular bone of WT ZOL and *Tcrd*$^{-/-}$ ZOL mice. *, $p < 0.05$; **, $p < 0.01$.

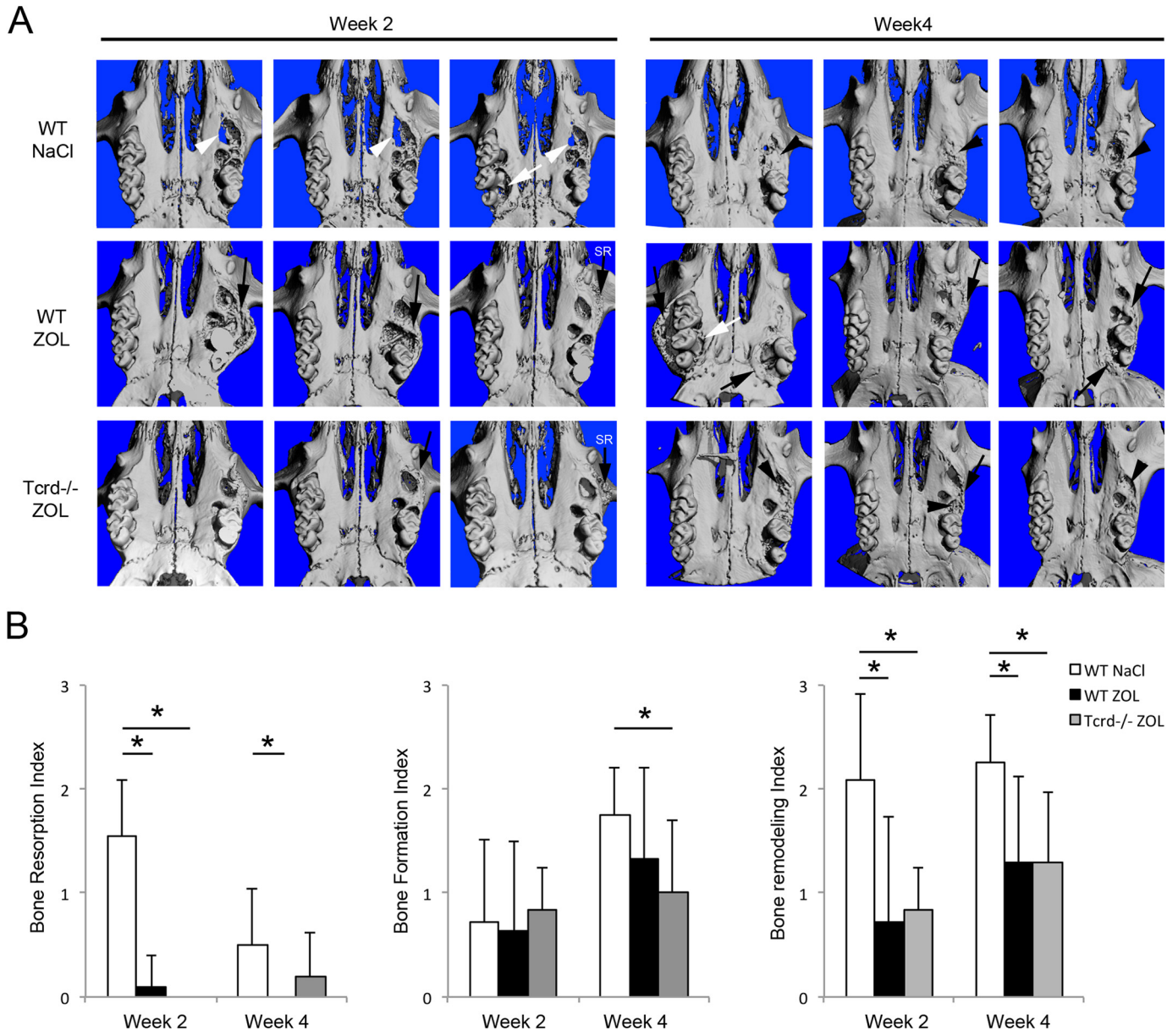

FIGURE 4. **Alveolar bone healing assessment by micro-CT imaging.** *A,* WT NaCl control mice exhibited signs of osteolysis at week 2 as roughened alveolar and palatal bone surfaces (*white arrowheads*). Bone formation within the extraction socket (*black arrowhead*) appeared to complete the wound healing process at week 4. We noted that one WT NaCl mouse exhibited periodontal disease at the nonextraction side (*white arrowhead*). In WT ZOL and *Tcrd*$^{-/-}$ ZOL mice, the evidence of bone resorption was not clearly observed, and the extraction socket was not completely filled by new bone formation (*black arrowheads*). Severe periosteal reaction (*black arrows*) was observed at the molar extraction site in 53% of the WT ZOL mice. A periosteal reaction was also noted in one WT ZOL mouse at the contralateral nonextraction side with periodontal disease (confirmed with histology). Although the severity of periosteal reaction in *Tcrd*$^{-/-}$ ZOL mice was much attenuated (*arrows*), the sun-ray type of calcified spikes was observed both in WT ZOL and *Tcrd*$^{-/-}$ ZOL mice (*SR with black arrow*). *B,* micro-CT images were used to rate bone formation (0–2) and bone resorption (0–2) appearance. The bone-remodeling rate was expressed by combining the rates of bone formation and resorption in each animal. Active bone remodeling was suggested in WT NaCl control mice. Both WT ZOL and *Tcrd*$^{-/-}$ ZOL mice showed significantly decreased bone resorption. *, $p < 0.05$.

T cells and h-CD3$^+$ T cells was 76.9 and 96.4%, respectively (Fig. 6*A*). After overnight activation by anti-CD3 antibody, anti-CD28 antibody, and rh-IL-2, T cells were co-cultured with ZOL-pretreated h-OC. The number of h-γδ T cells robustly increased during the co-culture period, whereas the number of h-CD3$^+$ T cells decreased (Fig. 6*B*).

After 6 days of co-culture, the secretion of IFN-γ was significantly higher by h-γδ T cells than h-CD3$^+$ T cells (Fig. 6*C*). The cell surface antigen analysis suggested that h-γδ T cells maintained the T cell profile with a small population of CD4$^+$ T cells. The large representation of CD69-positive staining indicated the lymphocyte activation (Fig. 6*D*). As such, this study suggested that h-γδ T cells were activated by ZOL-pretreated h-OCs.

Rag2$^{-/-}$ *Mice Engrafted with h-γδ T Cells*—One day after injection of h-γδ T cells to ZOL-treated *Rag2*$^{-/-}$ mice, the maxillary first molar was extracted. At the time of euthanasia 2 weeks after tooth extraction, spleen and bone marrow cells were harvested. The profile of endogenous mouse immune effectors showed the lack of CD3$^+$ T cells and CD19$^+$ B cells

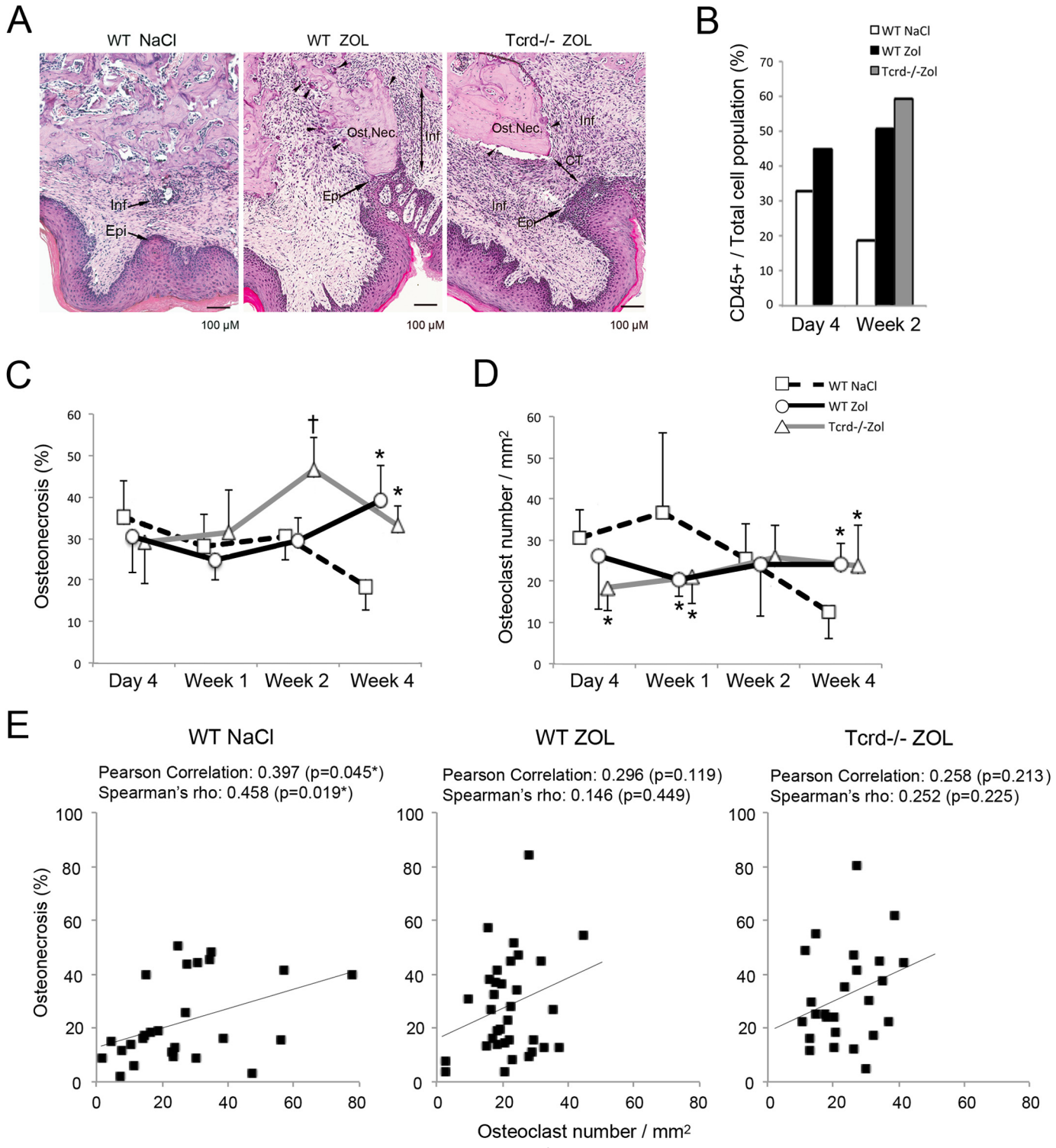

FIGURE 5. **Characterization of osteonecrosis in WT NaCl, WT ZOL, and *Tcrd*$^{-/-}$ ZOL mice.** *A,* localized inflammation (*Inf*) was evident near the surface of alveolar bone in WT NaCl mice. In WT ZOL mice, the intense inflammatory reaction was demonstrated in the oral mucosa (*double-headed arrow*; *Inf*). Abnormal epithelial tissue adhesion (*Epi*) was evident on the surface of partially necrotic alveolar bone (*Ost. Nec.*). In *Tcrd*$^{-/-}$ ZOL mice, inflammation was more diffused, and epithelial tissue did not reach the necrotic bone surface except at the pustule periphery. In both lesions, clusters of osteoclasts (*arrowheads*) were observed at and adjacent to the osteonecrosis site. *B,* CD45^{+} lymphocytes accounted for 30–45% of the dissociated cells from gingival/palatal tissue at day 4. The fraction of CD45^{+} cells decreased in WT NaCl mice at week 2. However, WT ZOL and *Tcrd*$^{-/-}$ ZOL mice exhibited similar fractions of CD45^{+} lymphocytes in the oral mucosa. *C,* area of osteonecrosis is presented as the percent of nonvital osteocytes over the total number of osteocytes on the oral side of palatal/alveolar bone. At week 4, the area of osteonecrosis was significantly larger in WT ZOL and *Tcrd*$^{-/-}$ ZOL mice than WT NaCl control mice. *D,* number of osteoclasts in the palatal/alveolar bone area suggested that the early increase in the tooth extraction wound of WT NaCl control mice followed by progressive decrease. Both WT ZOL and *Tcrd*$^{-/-}$ ZOL mice indicated a consistent appearance of osteoclasts throughout the experimental period, resulting in the elevated osteoclast number at week 4. *, $p < 0.05$; †, $p = 0.06$ compared with the WT NaCl control group. *E,* correlation between the osteonecrosis area and the number of OCs in week 1, week 2, and week 4 specimens. The WT NaCl group demonstrated the significant correlation between the osteonecrosis area and osteoclast number. By contrast, correlation pattern was similar in the WT ZOL and *Tcrd*$^{-/-}$ ZOL groups, which did not show statistical significance.

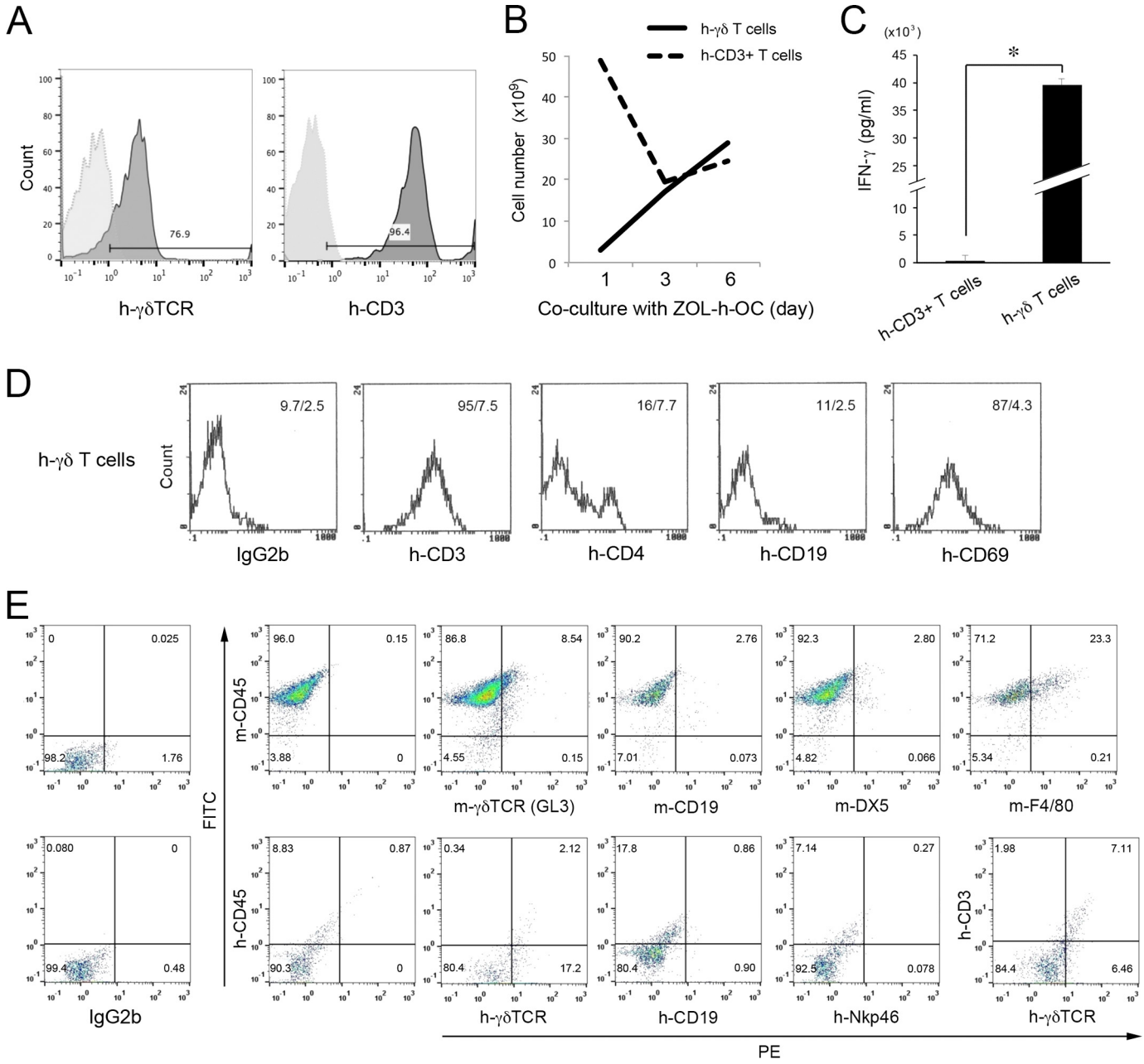

FIGURE 6. **h-γδ T cell activation through co-culture with ZOL-pretreated hOCs and engraftment to *Rag2*$^{-/-}$ ZOL mice.** *A,* positive selection of h-γδ T cells and h-CD3$^+$ T cells from peripheral blood samples from healthy donors resulted in 76.9 and 96.4% purities, respectively. *B,* number of h-γδ T cells increased during the co-culture period of 6 days with ZOL-pretreated h-OC, whereas the number of h-CD3$^+$ T cells decreased during the first 3 days. *C,* IFN-γ secreted by h-γδ T cells after the co-culture with h-OC was significantly higher than that of h-CD3+ T cells. *, $p < 0.01$. *D,* characterization of h-γδ T cells after the co-culture with ZOL-pretreated h-OC. h-γδ T cells were positive for CD3 and negative for CD19, indicating their T cell signature. Over 80% of h-γδ T cells showed CD69-positive, suggesting lymphocyte activation after co-culturing with ZOL-pretreated h-OC. *E,* representative profile of mouse immune effector cells in bone marrow of *Rag2*$^{-/-}$ ZOL mice engrafted with activated h-γδ T cells. The deficiency of mouse CD45$^+$ CD19$^+$ B cells and mouse CD45$^+$ γδTCR (GL3)$^+$ γδ T cells was indicated. Mouse CD45$^+$ cells contained F4/80$^+$ monocytes. Human cells appeared to be h-CD45$^+$ h-γδTCR$^+$ or h-CD3$^+$ h-γδTCR$^+$ suggesting the successful engraftment of h-γδ T cells.

but the presence of DX5$^+$ natural killer cells in spleen (data not shown) and F4/80$^+$ monocytes in bone marrow (Fig. 6*E*). The profile of human immune effectors indicated the presence of CD45$^+$γδTCR$^+$ and CD3$^+$γδTCR$^+$ cells (Fig. 6*E*), suggesting the successful engrafting of h-γδ T cells in *Rag2*$^{-/-}$ mice, which survived for the experimental period of 2 weeks.

Lack of ONJ-like Legions in ZOL-treated Rag2$^{-/-}$ *Mice—Rag2*$^{-/-}$mice with NaCl or ZOL injection showed accelerated tooth extraction wound healing as compared with WT mice. All *Rag2*$^{-/-}$ NaCl mice showed the closure of the tooth extraction wound at week 2 (Fig. 7*A*). Although *Rag2*$^{-/-}$ ZOL mice showed small food and debris impaction at the wound site in three out of five mice in the same healing period, histological examination revealed well healed extraction sockets (Fig. 7*A*).

Oral Epithelium Hyperplasia in Rag2$^{-/-}$ *ZOL Mice Engrafted with h-γδTCR—Rag2*$^{-/-}$ ZOL mice engrafted with h-γδ T cells showed an unusual roughened oral soft tissue healing at week 2 (Fig. 7*B*). Histological examination revealed vari-

ous degrees of oral epithelial hyperplasia in all mice. Oral epithelium exhibited irregular rete pegs and extensions of the basal cells. Where the hyperplastic oral epithelium embedded in the deep connective tissue, small food and debris were enclosed, and the tooth extraction socket showed the delay in bone healing (Fig. 7*B*).

In this project, we employed the autoclaved cellulose bedding for immunodeficient *Rag2*$^{-/-}$ mice, which might, in turn, change the wound-healing environment. WT NaCl mice housed in the same bedding environment showed the accelerated tooth extraction wound closure, whereas WT ZOL mice housed in autoclaved cellulose bedding demonstrated the ONJ

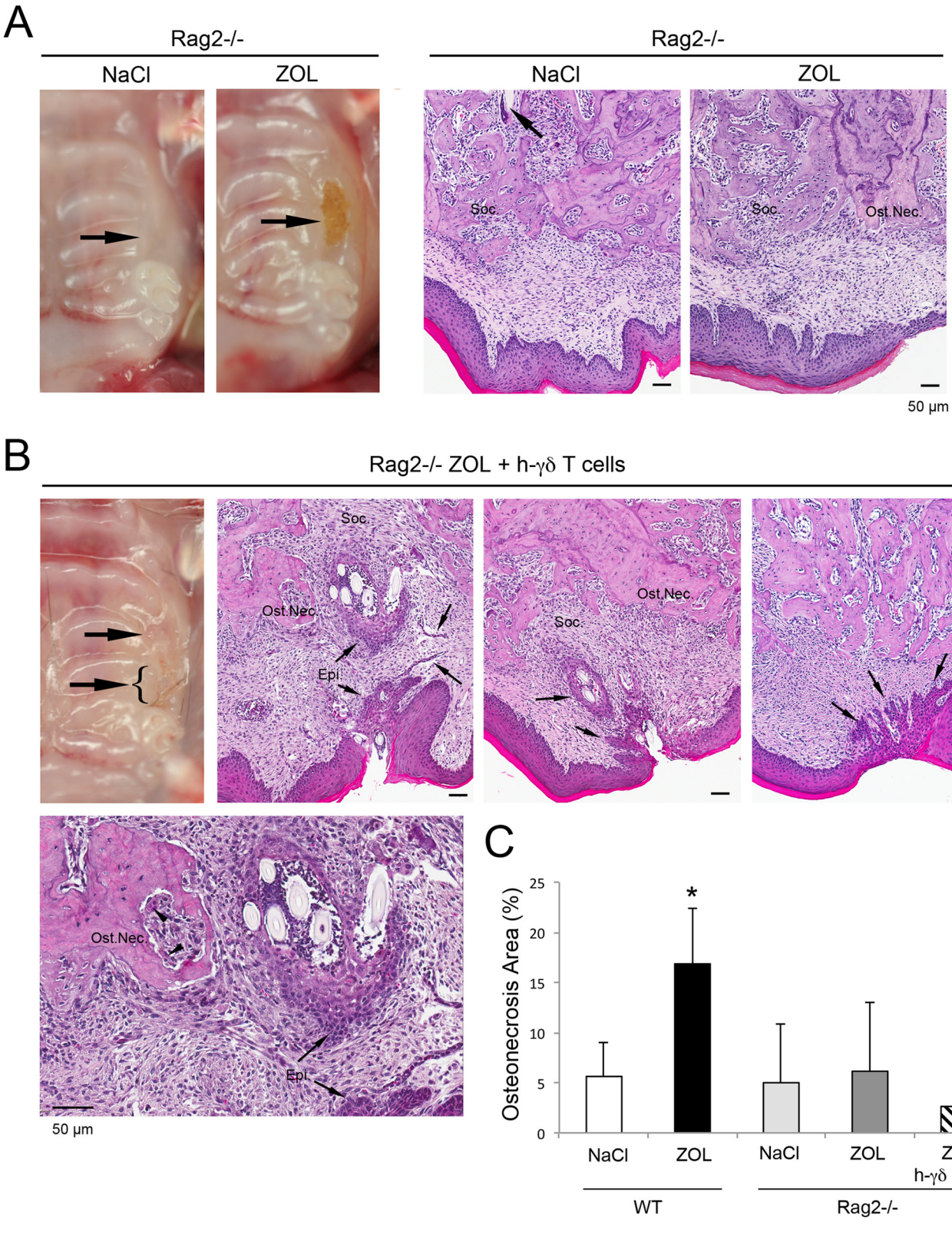

phenotype and oral wound was open at week 2 in all mice. WT ZOL mice showed the significantly larger osteonecrosis area than WT NaCl mice (Fig. 7*C*). The osteonecrosis area of *Rag2*$^{-/-}$ NaCl and *Rag2*$^{-/-}$ ZOL mice remained small at the level of WT NaCl mice. Despite the development of oral epithelial hyperplasia in h-γδ T cell-engrafted *Rag2*$^{-/-}$ ZOL mice, the osteonecrosis area remained unaffected (Fig. 7*C*).

Reduced Osteoclastogenesis in Rag2$^{-/-}$ *Mice—Rag2*$^{-/-}$ ZOL mice with or without h-γδ T cell engraftment demonstrated significantly less osteoclasts on the palatal bone surface than WT NaCl and WT ZOL mice (Fig. 8*A*). Dense inflammatory cell infiltration was observed in the palatal/gingival tissue of WT ZOL mice, which interfaced palatal bone lined by a number of osteoclasts. By contrast, no inflammatory infiltration was observed in *Rag2*$^{-/-}$ ZOL mice (Fig. 8*A*). Because the reduced osteoclast number was similarly observed in *Rag2*$^{-/-}$ NaCl mice (Fig. 8*A*), it was postulated that osteoclastogenesis on the palatal bone surface required the mediation by T cells, whereas the normalized osteoclast number in the extraction socket of *Rag2*$^{-/-}$ mice could be associated with the accelerated bone wound healing and remodeling.

m-OC Induced the Secretion of IFN-γ of h-γδ T Cells—The potential interaction between m-OC and h-γδ T cells was addressed by *in vitro* co-culture study. When h-γδ T cells were co-cultured with ZOL pretreated m-OC, IFN-γ secretion was significantly increased (Fig. 8*B*). Because m-OC alone did not secrete IFN-γ, activated h-γδ T cells were the source of IFN-γ. Surprisingly, IFN-γ secretion by h-γδ T cells was also increased when co-cultured with m-OC without ZOL pretreatment, albeit with a transient fashion (Fig. 8*B*). In the case of m-γδ T cells, nonspecific activation by m-OC with or without ZOL pretreatment was observed resulting in the higher levels of IFN-γ secretion (Fig. 8*B*).

Discussion

This study demonstrated the ONJ-like lesions with severe bone exposure (Fig. 1) and the nonexposure variants (Fig. 3) generated in mice that differed in the presence or absence of γδ T cells, respectively. WT ZOL mice exhibited extended exposure of partially necrotic alveolar bone associated with abnormal oral epithelial hyperplasia. By contrast, in the absence of γδ T cells, *Tcrd*$^{-/-}$ ZOL mice developed pustules on the surface of necrotic alveolar bone, which appeared to form fistulae with the oral epithelium. The exposure of necrotic bone has been a clinical hallmark of a fully developed ONJ lesion. However, the current position of the American Association of Oral and Maxillofacial Surgeons now includes intraoral or extraoral fistulae in the maxillofacial region as an additional clinical definition of medication-related ONJ (28). This revised ONJ definition underscores large clinical variations in the development of oral mucosa abnormalities in this disorder.

The area of osteonecrosis in WT ZOL mice progressively increased, whereas the osteonecrosis area in *Tcrd*$^{-/-}$ ZOL mice peaked at week 2 and then declined (Fig. 5*C*). The number of osteoclasts on the surface of palatal bone was equivalent in the WT ZOL and *Tcrd*$^{-/-}$ ZOL mice (Fig. 5*D*). However, histologically, osteoclasts appeared to cluster immediately outside the pustule in *Tcrd*$^{-/-}$ ZOL, resulting in bone sequestration (Fig. 3*C*). The bone sequestra in *Tcrd*$^{-/-}$ ZOL mice appeared to move toward the oral epithelium and was moved out to the oral cavity, which potentially contributed to the late reduction of the osteonecrotic area. In the presence of γδ T cells, osteoclasts in WT ZOL mice did not cluster but distributed on the palatal bone surface interfacing oral mucosa with severe inflammatory reaction (Fig. 8*A*). It was further noted that *Rag2*$^{-/-}$ mice lacking T and B cells showed the decreased osteoclast number on the palatal bone surface without inflammatory cell infiltration in the oral mucosa (Fig. 8*A*). Therefore, we postulate that tooth extraction-induced oral mucosa inflammation containing γδ T cells may be responsible, in part, for the induction of osteoclasts distributed on the palatal bone surface, although the severe inflammatory reaction in the form of pustule formation may be required for the localized osteoclast clustering in *Tcrd*$^{-/-}$ ZOL mice.

A recent retrospective analysis of BP-treated patients in Copenhagen concluded that the severe bone exposure and the nonexposure variants of ONJ belonged to the same disease condition. However, although the severe bone exposure variant was observed from the early BP treatment stage, the nonexposure variant was not reported until patients received repeated BP injections (35). ONJ patients who had received multiple injections of BP have been shown to develop deficiency of circulating γδ T cells (17). Human γδ T cells are largely composed of Vγ9Vδ2 T cells, which can react to phosphoantigens (pAg) such as bacteria or parasite-derived (*E*)-4-hydroxy-3-methyl-but-2-enyl pyrophosphate from the non-mevalonate pathway (36). Vγ9Vδ2 T cells can also react to mevalonate pathway-related pAgs such as IPP and isomer dimethylallyl pyrophosphate, albeit at much lower potencies (37, 38). Macrophages

FIGURE 7. **ONJ lesions of *Rag2*$^{-/-}$ mice and the effect of h-γδ T cell engraftment.** *A,* accelerated tooth extraction wound healing was observed in *Rag2*$^{-/-}$ mice. Two weeks after first molar extraction, both *Rag2*$^{-/-}$ NaCl and *Rag2*$^{-/-}$ ZOL mice exhibited uneventful healing (*arrows*) without oral mucosa swelling. Tooth extraction wound was completely closed in all *Rag2*$^{-/-}$ NaCl mice ($n = 5$), whereas *Rag2*$^{-/-}$ ZOL mice ($n = 5$) showed nonkeratinized oral mucosa covering the extraction socket or small open wound with food and debris impaction. Histologically, the extraction socket (*Soc*) was filled with newly formed bone in both *Rag2*$^{-/-}$ NaCl and *Rag2*$^{-/-}$ ZOL mice. The area of osteonecrosis (*Ost Nec*) was small. There were small food and debris impactions (*arrow*), which appeared to be integrated in the healed tissue. *B*, *Rag2*$^{-/-}$ ZOL mice engrafted with h-γδ T cells ($n = 4$) similarly showed the wound closure without swelling; however, there were unusual pits and irregular papilloma-like tissues (*arrows*) were present at the first molar extraction site. Histologically, all *Rag2*$^{-/-}$ ZOL h-γδ T cell mice exhibited various degrees of oral epithelial hyperplasia (*Epi*, *arrows*). In some specimens, epithelial "pouch" was found in the deep connective tissue, which often, but not always, contained small food and debris. The extraction socket (*Soc*) containing the epithelial pouch showed delayed bone formation. Osteonecrosis was found in small areas, associated with osteoclasts (*arrowheads*). *C,* osteonecrosis was determined by the bone area of containing ≥5 empty osteocyte lacunae over the total alveolar bone area. Because all *Rag2*$^{-/-}$ mice were housed with autoclaved cellulose-based bedding, a separate set of WT NaCl and WT ZOL mice ($n = 5$ in each group) was housed in the same environment after tooth extraction. Tooth extraction wound healing appeared to be more favorable in this environment; however, WT ZOL mice exhibited open tooth extraction wounds with significantly larger osteonecrosis areas. The osteonecrosis area of *Rag2*$^{-/-}$ ZOL mice remained small at the levels of WT NaCl and *Rag2*$^{-/-}$ NaCl mice. The engraftment of h-γδ T cells to *Rag2*$^{-/-}$ ZOL mice did not increase the osteonecrosis area. *, $p < 0.05$ compared with the WT NaCl control group.

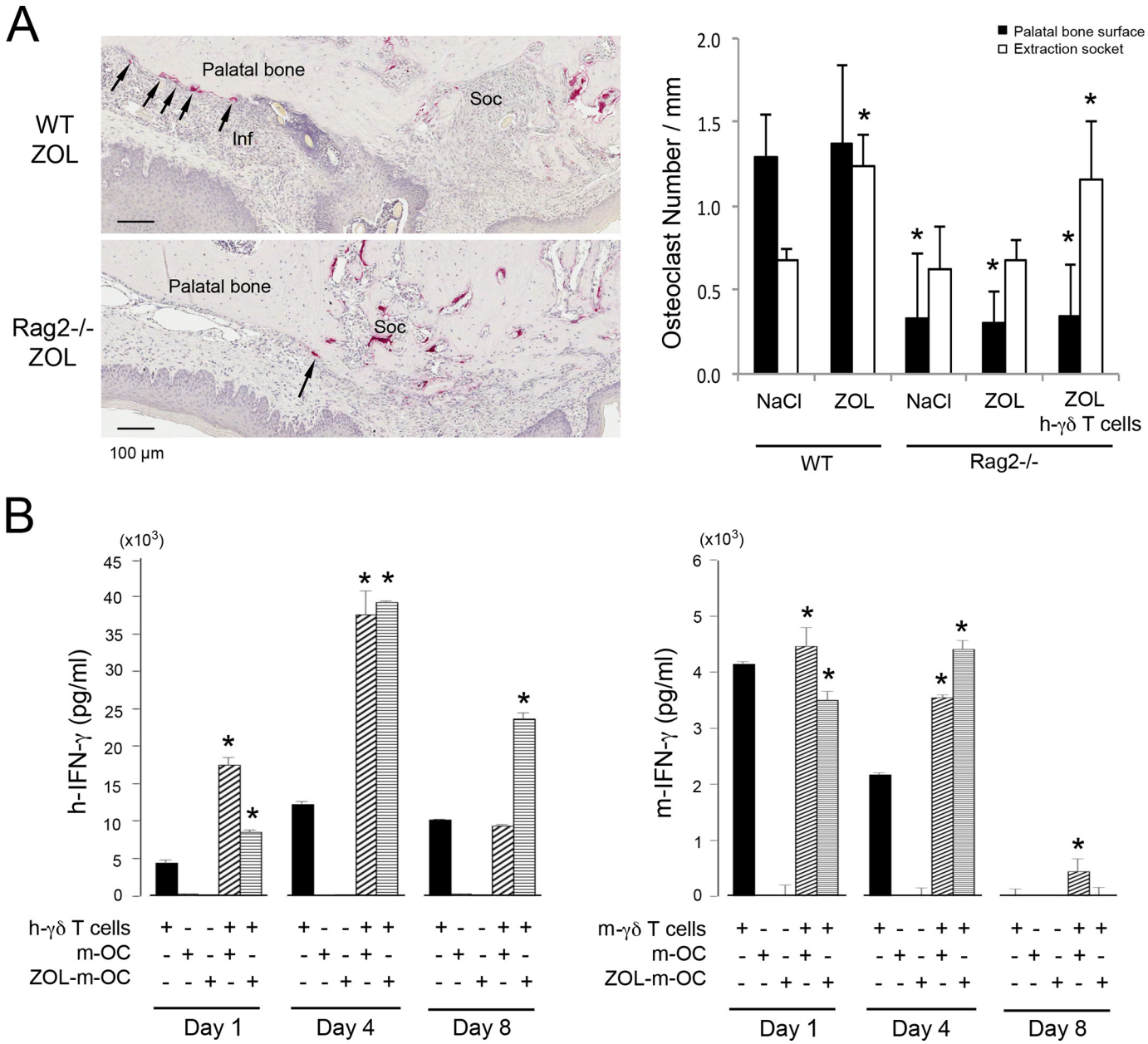

FIGURE 8. **Osteoclast behavior in *Rag2*$^{-/-}$ mice with h-γδ T cell engraftment.** *A,* tartrate-resistant acid phosphatase staining revealed osteoclasts on the surface of palatal bone (*arrows*) interfacing the area of oral mucosa inflammation (*Inf*) in WT ZOL mice. Strikingly, osteoclasts on the palatal surface were nearly absent in *Rag2*$^{-/-}$ ZOL mice, whereas osteoclasts appeared in the bone remodeling area of tooth extraction socket (*Soc*). The number of osteoclasts normalized by the bone surface was significantly reduced on the palatal bone surface in *Rag2*$^{-/-}$ regardless of ZOL treatment as well as h-γδ T cell engraftment. The osteoclast number in the extraction socket was normalized in *Rag2*$^{-/-}$ NaCl and *Rag2*$^{-/-}$ ZOL mice, whereas h-γδ T cell-engrafted mice remained high. *, $p < 0.05$ compared with the WT NaCl control group. *B,* stimulatory effect of m-OC on h-γδ T cells and m-γδ T cells was assessed *in vitro*. ELISA revealed that m-OC with ZOL pretreatment specifically activated the IFN-γ secretion by h-γδ T cells but not by m-γδ T cell. However, nonspecific activation by m-OC was observed in both h-γδ T cells and m-γδ T cells, which secreted higher levels of IFN-γ. *, $p < 0.05$ compared with the h-γδ T cell or m-γδ T cell alone group at each time point.

exposed to BP such as ZOL become an activator of Vγ9Vδ2 T cells, likely in consequence of intracellular IPP accumulation. The repeated BP injections are postulated to result in the repeated activation of Vγ9Vδ2 T cells leading to eventual γδ T cell depletion (17, 18). It is tempting to speculate that the decreased circulating Vγ9Vδ2 T cells may causally associate with the development of nonexposure and fistula phenotype of ONJ in humans.

It has been established that the Vγ9Vδ2 T cell receptor as well as butyrophilin-3A1 critical for IPP-induced activation of γδ T cells are conserved only in humans, primates, and a few other placental animals but not in mice (39, 40). Therefore, mouse γδ T cells do not respond to pAgs, and the ZOL injection should not activated the circulating γδ T cells in mice through a similar mechanism as in humans. Thus, this study examined the role of human γδ T cells in the development of oral mucosal phenotypes in ZOL-treated *Rag2*$^{-/-}$ mice. Like BP-exposed macrophages, this study demonstrated that ZOL-treated h-OCs activated h-γδ T cells. By co-culturing with ZOL-pretreated h-OC, h-γδ T cells were found to increase the cell

counts, secrete IFN-γ at a much higher level than the similarly activated h-CD3$^+$ T cells, and express the lymphocyte activation marker CD69 (Fig. 6). When h-γδ T cells that were pre-activated by ZOL-treated h-OCs were engrafted onto *Rag2*$^{-/-}$ ZOL mice, the tooth extraction wound healed with abnormal oral epithelial hyperplasia (Fig. 7).

The abnormal oral epithelial hyperplasia referred to as pseudoepitheliomatous hyperplasia (PEH) was reported in 60% of human ONJ biopsy specimens (24, 31) and was associated with the more aggressive ONJ phenotype with necrotic bone exposure. Akilov *et al.* (41) reported the development of PEH in mouse ear skin by the injection of TNF-α and IFN-γ, suggesting that overproduction of Th1 cytokines in the barrier immunity stimulated the unregulated proliferation and migration of epidermal basal cells. *Rag2*$^{-/-}$ mice used in this study lacked T and B cells, whereas NK cells and monocytes were present (Fig. 6). Therefore, the engrafted h-γδ T cells were likely to be a source of Th1 cytokines such as TNF-α and IFN-γ (42).

This study demonstrated that PEH-like oral epithelial migration was less apparent in *Tcrd*$^{-/-}$ ZOL mice that nonetheless developed the nonexposure variant-like ONJ lesion (Fig. 4). Conversely, the prolonged retention of γδ T cells in the tooth extraction wound of WT ZOL mice may have contributed to PEH-like oral epithelial hyperplasia leading to the gross exposure of necrotic bone and the severe ONJ phenotype.

To better understand the "γδ T cell humanized" mice, h-γδ T cells and m-γδ T cells were co-cultured with mouse OC (m-OC). As expected, the activation of h-γδ T cells was observed with ZOL pretreated m-OC. However, co-culturing with m-OC without ZOL pretreatment also activated h-γδ T cells. The ZOL treatment of m-OC is expected to accumulate pAg such as IPP, which specifically activate h-γδ T cells. However, the surprising observation of h-γδ T cell activation by ZOL-untreated m-OC, albeit with a transient nature, should suggest a nonspecific activation of immune effectors by OCs. The activation of m-γδ T cells by m-OC with or without ZOL pretreatment further supports the previously unrecognized functions of OCs other than bone resorption, which might include regulatory roles of local immune effectors. Besides the pAg-derived activation, human and mouse γδ T cells are activated by peptide stimulants such as NKG2D ligands (43). It is tempting to speculate that ONJ pathogenesis may involve nonspecific activation of γδ T cells by OCs through the non-pAg activation mechanism in mice as well as in humans.

It is important to report that *Rag2*$^{-/-}$ ZOL mice with or without h-γδ T cell engraftment did not develop osteonecrosis (Fig. 7), whereas WT ZOL and *Tcrd*$^{-/-}$ ZOL developed osteonecrosis (Figs. 1, 3, and 5). It appears that the prolonged or unresolved oral inflammation is commonly observed in our mouse models as well as in ONJ patients. The time course profile of OC numbers at the surface of jawbone was similarly sustained in WT ZOL and *Tcrd*$^{-/-}$ ZOL mice (Fig. 5). By contrast, *Rag2*$^{-/-}$ mice lacking oral mucosal inflammation significantly reduced the recruitment of osteoclasts (Fig. 8*A*). Considering the mode of action of BP targeting OCs, it may not be a mere coincidence that osteonecrosis legions were found to localize with or adjacent to a cluster of OCs (Fig. 3*C*). Therefore, the lack of OC in *Rag2*$^{-/-}$ ZOL mice may lead to the lack of osteonecrosis.

We previously proposed that ZOL-affected OCs might mediate the pro-inflammatory environment in oral mucosa based on the unique observation of a group of inflammatory cells closely associated with OCs in rat jawbones treated with ZOL (24). This study further suggested the role of OC on the immune regulation (Fig. 8*B*). Zhang *et al.* (44) demonstrated an unusually increased number of IL17-expressing helper T cells and M1 macrophages in the oral mucosa of ONJ patients. The ONJ patient demography with co-morbidities such as diabetes type 2 (45) may suggest the presence of systemic pro-inflammatory susceptibility. As such, the dysregulation of systemic as well as local oral mucosa immunity may provide the underlining core mechanism to the prolonged oral inflammation leading to the development of ONJ, in which γδ T cells may modify the oral epithelial disease phenotype.

Author Contributions—I. N., S. P., and A. J. designed this study. S. P., K. K., K. K., H. H. T., S. B., D. T. Q., A. J., and I. N. performed the experiments. S. P., J. W. S., A. J., and I. N. analyzed and interpreted the data. I. N. and A. J. drafted the manuscript. All authors agreed on the content of the manuscript. I. N. accepts responsibility for the integrity of the data analysis.

Acknowledgments—We thank Dr. Mitchell Kronenberg of the La Jolla Institute for Allergy and Immunity, La Jolla, CA, and Dr. Wendy Havran of the Scripps Research Institute, La Jolla, CA, for their guidance on the research strategies used in this study. We also thank Dr. Anna Kozlowska, Weintraub Center for Reconstructive Biotechnology, UCLA School of Dentistry, for immunological data interpretation, and Dr. Toshiaki Shibutani of the Asahi University School of Dentistry for the generous support. Histopathological and immunohistological specimens were prepared at the Tissue Procurement Core Laboratory, Department of Pathology and Laboratory Medicine, David Geffen School of Medicine at UCLA.

References

1. Reid, I. R., and Cornish, J. (2012) Epidemiology and pathogenesis of osteonecrosis of the jaw. *Nat. Rev. Rheumatol.* **8,** 90–96
2. Saad, F., Brown, J. E., Van Poznak, C., Ibrahim, T., Stemmer, S. M., Stopeck, A. T., Diel, I. J., Takahashi, S., Shore, N., Henry, D. H., Barrios, C. H., Facon, T., Senecal, F., Fizazi, K., Zhou, L., *et al.* (2012) Incidence, risk factors, and outcomes of osteonecrosis of the jaw: integrated analysis from three blinded active-controlled phase III trials in cancer patients with bone metastases. *Ann. Oncol.* **23,** 1341–1347
3. Khosla, S., Burr, D., Cauley, J., Dempster, D. W., Ebeling, P. R., Felsenberg, D., Gagel, R. F., Gilsanz, V., Guise, T., Koka, S., McCauley, L. K., McGowan, J., McKee, M. D., Mohla, S., Pendrys, D. G., *et al.* (2007) Bisphosphonate-associated osteonecrosis of the jaw: report of a task force of the American Society for Bone and Mineral Research. *J. Bone Miner. Res.* **22,** 1479–1491
4. Ruggiero, S. L., Dodson, T. B., Assael, L. A., Landesberg, R., Marx, R. E., and Mehrotra, B. (2009) American Association of Oral and Maxillofacial Surgeons position paper on bisphosphonate-related osteonecrosis of the jaws–2009 update. *J. Oral Maxillofac. Surg.* **67,** 2–12
5. Cetiner, S., Sucak, G. T., Kahraman, S. A., Aki, S. Z., Kocakahyaoglu, B., Gultekin, S. E., Cetiner, M., and Haznedar, R. (2009) Osteonecrosis of the jaw in patients with multiple myeloma treated with zoledronic acid. *J. Bone Miner. Metab.* **27,** 435–443
6. Ruggiero, S. L., Mehrotra, B., Rosenberg, T. J., and Engroff, S. L. (2004) Osteonecrosis of the jaws associated with the use of bisphosphonates: a

review of 63 cases. *J. Oral Maxillofac. Surg.* **62,** 527–534
7. Mavrokokki, T., Cheng, A., Stein, B., and Goss, A. (2007) Nature and frequency of bisphosphonate-associated osteonecrosis of the jaws in Australia. *J. Oral Maxillofac. Surg.* **65,** 415–423
8. Coleman, R., Woodward, E., Brown, J., Cameron, D., Bell, R., Dodwell, D., Keane, M., Gil, M., Davies, C., Burkinshaw, R., Houston, S. J., Grieve, R. J., Barrett-Lee, P. J., and Thorpe, H. (2011) Safety of zoledronic acid and incidence of osteonecrosis of the jaw (ONJ) during adjuvant therapy in a randomised phase III trial (AZURE: BIG 01–04) for women with stage II/III breast cancer. *Breast Cancer Res. Treat.* **127,** 429–438
9. Coleman, R. E., Marshall, H., Cameron, D., Dodwell, D., Burkinshaw, R., Keane, M., Gil, M., Houston, S. J., Grieve, R. J., Barrett-Lee, P. J., Ritchie, D., Pugh, J., Gaunt, C., Rea, U., Peterson, J., *et al.* (2011) Breast-cancer adjuvant therapy with zoledronic acid. *N. Engl. J. Med.* **365,** 1396–1405
10. Woo, S. B., Hellstein, J. W., and Kalmar, J. R. (2006) Narrative (corrected) review: bisphosphonates and osteonecrosis of the jaws. *Ann. Intern. Med.* **144,** 753–761
11. Ngamphaiboon, N., Frustino, J. L., Kossoff, E. B., Sullivan, M. A., and O'Connor, T. L. (2011) Osteonecrosis of the jaw: dental outcomes in metastatic breast cancer patients treated with bisphosphonates with/without bevacizumab. *Clin. Breast Cancer* **11,** 252–257
12. Smidt-Hansen, T., Folkmar, T. B., Fode, K., Agerbaek, M., and Donskov, F. (2013) Combination of zoledronic acid and targeted therapy is active but may induce osteonecrosis of the jaw in patients with metastatic renal cell carcinoma. *J. Oral Maxillofac. Surg.* **71,** 1532–1540
13. Miyazaki, H., Nishimatsu, H., Kume, H., Suzuki, M., Fujimura, T., Fukuhara, H., Enomoto, Y., Ishikawa, A., Igawa, Y., Hirano, Y., and Homma, Y. (2012) Leukopenia as a risk factor for osteonecrosis of the jaw in metastatic prostate cancer treated using zoledronic acid and docetaxel. *BJU Int.* **110,** E520–E525
14. Presland, R. B., and Jurevic, R. J. (2002) Making sense of the epithelial barrier: what molecular biology and genetics tell us about the functions of oral mucosal and epidermal tissues. *J. Dent. Educ.* **66,** 564–574
15. Kyrgidis, A., Vahtsevanos, K., Koloutsos, G., Andreadis, C., Boukovinas, I., Teleioudis, Z., Patrikidou, A., and Triaridis, S. (2008) Bisphosphonate-related osteonecrosis of the jaws: a case-control study of risk factors in breast cancer patients. *J. Clin. Oncol.* **26,** 4634–4638
16. Barasch, A., Cunha-Cruz, J., Curro, F. A., Hujoel, P., Sung, A. H., Vena, D., Voinea-Griffin, A. E., CONDOR Collaborative Group, Beadnell, S., Craig, R. G., DeRouen, T., Desaranayake, A., Gilbert, A., Gilbert, G. H., Goldberg, K., *et al.* (2011) Risk factors for osteonecrosis of the jaws: a case-control study from the CONDOR dental PBRN. *J. Dent. Res.* **90,** 439–444
17. Kalyan, S., Quabius, E. S., Wiltfang, J., Mönig, H., and Kabelitz, D. (2013) Can peripheral blood γδ T cells predict osteonecrosis of the jaw? An immunological perspective on the adverse drug effects of aminobisphosphonate therapy. *J. Bone Miner. Res.* **28,** 728–735
18. Rossini, M., Adami, S., Viapiana, O., Fracassi, E., Ortolani, R., Vella, A., Zanotti, R., Tripi, G., Idolazzi, L., and Gatti, D. (2012) Long-term effects of amino-bisphosphonates on circulating γδ T cells. *Calcif. Tissue Int.* **91,** 395–399
19. Havran, W. L. (2000) A role for epithelial γδ T cells in tissue repair. *Immunol. Res.* **21,** 63–69
20. Havran, W. L., and Jameson, J. M. (2010) Epidermal T cells and wound healing. *J. Immunol.* **184,** 5423–5428
21. Yardeni, T., Eckhaus, M., Morris, H. D., Huizing, M., and Hoogstraten-Miller, S. (2011) Retro-orbital injections in mice. *Lab. Anim.* **40,** 155–160
22. Hunter, R. P., and Isaza, R. (2008) Concepts and issues with interspecies scaling in zoological pharmacology. *J. Zoo Wildl. Med.* **39,** 517–526
23. Ting, K., Ramachandran, H., Chung, K. S., Shah-Hosseini, N., Olsen, B. R., and Nishimura, I. (1999) A short isoform of Col9a1 supports alveolar bone repair. *Am. J. Pathol.* **155,** 1993–1999
24. Hokugo, A., Christensen, R., Chung, E. M., Sung, E. C., Felsenfeld, A. L., Sayre, J. W., Garrett, N., Adams, J. S., and Nishimura, I. (2010) Increased prevalence of bisphosphonate-related osteonecrosis of the jaw with vitamin D deficiency in rats. *J. Bone Miner. Res.* **25,** 1337–1349
25. Prinz, I., Sansoni, A., Kissenpfennig, A., Ardouin, L., Malissen, M., and Malissen, B. (2006) Visualization of the earliest steps of γδ T cell development in the adult thymus. *Nat. Immunol.* **7,** 995–1003
26. Jewett, A., Cavalcanti, M., Giorgi, J., and Bonavida, B. (1997) Concomitant killing in vitro of both gp120-coated $CD4^+$ peripheral T lymphocytes and natural killer cells in the antibody-dependent cellular cytotoxicity (ADCC) system. *J. Immunol.* **158,** 5492–5500
27. Itohara, S., Mombaerts, P., Lafaille, J., Iacomini, J., Nelson, A., Clarke, A. R., Hooper, M. L., Farr, A., and Tonegawa, S. (1993) T cell receptor delta gene mutant mice: independent generation of αβ T cells and programmed rearrangements of γδ TCR genes. *Cell* **72,** 337–348
28. Ruggiero, S. L., Dodson, T. B., Fantasia, J., Goodday, R., Aghaloo, T., Mehrotra, B., O'Ryan, F., American Association of Oral and Maxillofacial Surgeons. (2014) American Association of Oral and Maxillofacial Surgeons position paper on medication-related osteonecrosis of the jaw–2014 update. *J. Oral Maxillofac. Surg.* **72,** 1938–1956
29. Hemingway, F., Cheng, X., Knowles, H. J., Estrada, F. M., Gordon, S., and Athanasou, N. A. (2011) *In vitro* generation of mature human osteoclasts. *Calcif. Tissue Int.* **89,** 389–395
30. Hao, Z., and Rajewsky, K. (2001) Homeostasis of peripheral B cells in the absence of B cell influx from the bone marrow. *J. Exp. Med.* **194,** 1151–1164
31. Hansen, T., Kunkel, M., Weber, A., and James Kirkpatrick, C. (2006) Osteonecrosis of the jaws in patients treated with bisphosphonates-histomorphologic analysis in comparison with infected osteoradionecrosis. *J. Oral Pathol. Med.* **35,** 155–160
32. Bedogni, A., Blandamura, S., Lokmic, Z., Palumbo, C., Ragazzo, M., Ferrari, F., Tregnaghi, A., Pietrogrande, F., Procopio, O., Saia, G., Ferretti, M., Bedogni, G., Chiarini, L., Ferronato, G., Ninfo, V., *et al.* (2008) Bisphosphonate-associated jawbone osteonecrosis: a correlation between imaging techniques and histopathology. *Oral Surg. Oral Med. Oral Pathol. Oral Radiol. Endod.* **105,** 358–364
33. Morag, Y., Morag-Hezroni, M., Jamadar, D. A., Ward, B. B., Jacobson, J. A., Zwetchkenbaum, S. R., and Helman, J. (2009) Bisphosphonate-related osteonecrosis of the jaw: a pictorial review. *Radiographics* **29,** 1971–1984
34. Roelofs, A. J., Coxon, F. P., Ebetino, F. H., Lundy, M. W., Henneman, Z. J., Nancollas, G. H., Sun, S., Blazewska, K. M., Bala, J. L., Kashemirov, B. A., Khalid, A. B., McKenna, C. E., and Rogers, M. J. (2010) Fluorescent risedronate analogues reveal bisphosphonate uptake by bone marrow monocytes and localization around osteocytes *in vivo*. *J. Bone Miner. Res.* **25,** 606–616
35. Schiodt, M., Reibel, J., Oturai, P., and Kofod, T. (2014) Comparison of nonexposed and exposed bisphosphonate-induced osteonecrosis of the jaws: a retrospective analysis from the Copenhagen cohort and a proposal for an updated classification system. *Oral Surg. Oral Med. Oral Pathol. Oral. Radiol.* **117,** 204–213
36. Eberl, M., and Moser, B. (2009) Monocytes and γδ T cells: close encounters in microbial infection. *Trends Immunol.* **30,** 562–568
37. Kunzmann, V., Bauer, E., Feurle, J., Weissinger, F., Tony, H. P., and Wilhelm, M. (2000) Stimulation of γδ T cells by aminobisphosphonates and induction of antiplasma cell activity in multiple myeloma. *Blood* **96,** 384–392
38. Wilhelm, M., Kunzmann, V., Eckstein, S., Reimer, P., Weissinger, F., Ruediger, T., and Tony, H. P. (2003) γδ T cells for immune therapy of patients with lymphoid malignancies. *Blood* **102,** 200–206
39. Karunakaran, M. M., Göbel, T. W., Starick, L., Walter, L., and Herrmann, T. (2014) Vγ9 and Vδ2 T cell antigen receptor genes and butyrophilin 3 (BTN3) emerged with placental mammals and are concomitantly preserved in selected species like alpaca (*Vicugna pacos*). *Immunogenetics* **66,** 243–254
40. Karunakaran, M. M., and Herrmann, T. (2014) The Vγ9Vδ2 T cell antigen receptor and butyrophilin-3 A1: models of interaction, the possibility of co-evolution, and the case of dendritic epidermal T cells. *Front. Immunol.* **5,** 648
41. Akilov, O. E., Donovan, M. J., Stepinac, T., Carter, C. R., Whitcomb, J. P., Hasan, T., and McDowell, M. A. (2007) T helper type 1 cytokines and keratinocyte growth factor play a critical role in pseudoepitheliomatous hyperplasia initiation during cutaneous leishmaniasis. *Arch. Dermatol. Res.* **299,** 315–325
42. Inoue, S., Niikura, M., Mineo, S., and Kobayashi, F. (2013) Roles of IFN-γ and γδ T cells in protective immunity against blood-stage malaria. *Front.*

Immunol. **4,** 258
43. Ibusuki, A., Kawai, K., Yoshida, S., Uchida, Y., Nitahara-Takeuchi, A., Kuroki, K., Kajikawa, M., Ose, T., Maenaka, K., Kasahara, M., and Kanekura, T. (2014) NKG2D triggers cytotoxicity in murine epidermal γδ T cells via PI3K-dependent, Syk/ZAP70-independent signaling pathway. *J. Invest. Dermatol.* **134,** 396–404
44. Zhang, Q., Atsuta, I., Liu, S., Chen, C., Shi, S., Shi, S., and Le, A. D. (2013) IL-17-mediated M1/M2 macrophage alteration contributes to pathogenesis of bisphosphonate-related osteonecrosis of the jaws. *Clin. Cancer Res.* **19,** 3176–3188
45. Khamaisi, M., Regev, E., Yarom, N., Avni, B., Leitersdorf, E., Raz, I., and Elad, S. (2007) Possible association between diabetes and bisphosphonate-related jaw osteonecrosis. *J. Clin. Endocrinol. Metab.* **92,** 1172–1175
46. Kuroshima, S., and Yamashita, J. (2013) Chemotherapeutic and antiresorptive combination therapy suppressed lymphangiogenesis and induced osteonecrosis of the jaw-like lesions in mice. *Bone* **56,** 101–109
47. Kikuiri, T., Kim, I., Yamaza, T., Akiyama, K., Zhang, Q., Li, Y., Chen, C., Chen, W., Wang, S., Le, A. D., and Shi, S. (2010) Cell-based immunotherapy with mesenchymal stem cells cures bisphosphonate-related osteonecrosis of the jaw-like disease in mice. *J. Bone Miner. Res.* **25,** 1668–1679
48. Bi, Y., Gao, Y., Ehirchiou, D., Cao, C., Kikuiri, T., Le, A., Shi, S., and Zhang, L. (2010) Bisphosphonates cause osteonecrosis of the jaw-like disease in mice. *Am. J. Pathol.* **177,** 280–290
49. Zhao, Y., Wang, L., Liu, Y., Akiyama, K., Chen, C., Atsuta, I., Zhou, T., Duan, X., Jin, Y., and Shi, S. (2012) Technetium-99 conjugated with methylene diphosphonate ameliorates ovariectomy-induced osteoporotic phenotype without causing osteonecrosis in the jaw. *Calcif. Tissue Int.* **91,** 400–408
50. Kang, B., Cheong, S., Chaichanasakul, T., Bezouglaia, O., Atti, E., Dry, S. M., Pirih, F. Q., Aghaloo, T. L., and Tetradis, S. (2013) Periapical disease and bisphosphonates induce osteonecrosis of the jaws in mice. *J. Bone Miner. Res.* **28,** 1631–1640
51. Kobayashi, Y., Hiraga, T., Ueda, A., Wang, L., Matsumoto-Nakano, M., Hata, K., Yatani, H., and Yoneda, T. (2010) Zoledronic acid delays wound healing of the tooth extraction socket, inhibits oral epithelial cell migration, and promotes proliferation and adhesion to hydroxyapatite of oral bacteria, without causing osteonecrosis of the jaw, in mice. *J. Bone Miner. Metab.* **28,** 165–175